Terminal Transient For Minimum-Time Dash Mission

by

William D. Lightsey

Thesis submitted to the Faculty of the

Virginia Polytechnic Institute and State University

in partial fulfillment of the requirements for the degree of

Master of Science

in

Aerospace Engineering

APPROVED:

Henry J. Kelley, Chairman

Frederick H. Lutze

Eugene M. Cliff

March 1987

Blacksburg, Virginia

Terminal Transient For Minimum-Time Dash Mission

by

William D. Lightsey

Henry J. Kelley, Chairman

Aerospace Engineering

(ABSTRACT)

The terminal stage of a minimum-time dash mission of a high-performance aircraft is studied using both a reduced-order "energy" model formulation and a point-mass model formulation of the aircraft.

The mission is confined to vertical plane maneuvers, and is defined as consisting of three stages; a climb to the dash point, a steady-state dash at the high velocity point, and finally, a terminal transient from the dash point to the final state. This terminal maneuver evolves outside of the flight envelope, rapidly decreasing altitude while increasing the velocity to values greater than the dash velocity. The velocity then decreases from this maximum value as required in order to meet the final state specification.

Some of the trajectories that are generated during this terminal transient maneuver experience dynamic pressures that will exceed the dynamic pressure limit unless a constraint is placed on the state variables. Because of the need for enforcing this state constraint, a direct adjoining method for handling state constraints in the optimal control problem is studied. A numerical example is given to demonstrate the application of this method of handling state constraints for the case of the dynamic pressure limit.

Finally, trajectories are generated that lead from the dash point to a final state having lower altitude and energy values than those of the dash point, and observations are made concerning the characteristics of these maneuvers.

Acknowledgments

I would like to thank Dr. E.M. Cliff for his help and guidance, and his willingness to discuss at any time the problems that I encountered during this work. I would like to thank Dr. H.J. Kelley for his help and guidance and for serving as chairman of my advisory committee. Also, I would like to thank Dr. F.H. Lutze for serving on my committee and for his valuable help in solving the state constraint problems.

I would like to thank my friends and for the constant help that they gave me in solving problems throughout the course of this research. Also, I would like especially to thank for his valuable help in the early stages of this work and for his great contribution to the energy model work.

Table of Contents

List of Symbols

C ..... vector of tangency conditions

C_{Do} ..... zero lift drag coefficient

C_{Di} ..... induced drag coefficient

C_L ..... lift coefficient

D ..... total drag

D_o ..... zero lift drag

D_i ..... induced drag

E ..... specific energy

g ..... acceleration of gravity

h ..... altitude

H ..... Hamiltonian

$\bar{H}$ ..... augmented Hamiltonian

L ..... lift

M ..... Mach number

$\overline{M}$ ..... Mach limit

N ..... load factor

Q .....dynamic pressure

$\overline{Q}$ .....dynamic pressure limit

Q_f.....fuel flow rate

S .....state constraint

S_r .....wing reference area

T.....thrust

t.....flight time

t_1.....entry time of constrained arc

t_2.....exit time of constrained arc

V.....velocity

W.....weight of aircraft

W_f.....weight of fuel

X .....down range

Y.....cross range

Greek symbols

β_i.....array of state constraints

γ .....flight path angle

ε.....interpolation parameter

η .....throttle control variable

$\lambda_{(\ )}$..... costate variable

μ .....state constraint multiplier

π .....multiplier for jumps in costates

ρ .....air density

φ .....bank angle

χ .....heading angle

Superscripts

T.....transpose

+.....after an event

−.....before an event

$(\dot{\ })$.....derivative with respect to time

Subscripts

d .....value at dash point

s.....value at throttle switching point

List of Figures

1 Introduction

1.1 Minimum-Time Trajectories

Several studies have been reported in the literature on various formulations of minimum-time trajectory calculations for atmospheric flight. Such problems as minimum-time turns and minimum-time vertical maneuvers such as the "half-loop" and "split-S" have been analyzed.[36] One such problem that arises in aircraft performance is that of minimum time-to-climb from low altitude to a given point inside the level flight envelope. A particularly interesting trajectory of this sort is the one leading from low altitude horizontal flight to the high velocity point on the flight envelope. This would form the initial stage of a minimum-time dash mission where the range to be covered is quite long. The aircraft would climb to the dash point and then remain there until the specified range is covered. Studies of various formulations of these minimum-time problems have appeared in the literature.

Suppose now that, in addition to having a very large range to cover, the final altitude and velocity specified is lower than the altitude and velocity at the dash-point. The

minimum-time trajectory would lead from the deck to the dash-point, remain at the dash-point for some time, and, then, some terminal maneuver would be required to move from the dash-point to the specified end conditions. This terminal maneuver from the dash-point to final points having lower altitude and velocity than the dash-point is the focus of this study.

A brief discussion of this terminal transient for a reduced-order "energy" model formulation is given by Weston [22], but no detailed investigation is carried out there. Some mention of a terminal stage is also given by Bryson, Desai, and Hoffman [3]. Here an "energy" model is also used to generate maximum-range trajectories that climb to some altitude and Mach number and then dive to a final state having a lower altitude and Mach number. No dynamic pressure constraint or Mach limit is considered, so the trajectories dive to zero altitude. In ref [40], trajectories are generated that climb, cruise, and descend, but here the problem is oriented toward commercial airline applications. The performance index is devised as a linear combination of time and fuel. The thrust is constrained in order to obtain the desired operation. Because of the commercial-airline application, the terminal transient does not experience any excessive Mach numbers or dynamic pressures, so these state constraints are not considered.

1.2 State Constraints

For a realistic study of this terminal transient, any state constraints that may be encountered must be considered in the problem formulation. Figure 1 shows the level flight envelope for the aircraft data used in the present study and the constraints imposed on the state variables. As many as three of these constraints could be encountered by a terminal path leading from the dash-point to low energy. The terminal

trajectory could possibly ride the Mach limit for some time, then encounter the dynamic pressure constraint, and after riding it for some time, encounter the terrain limit.[22] In the present model, the Mach number at the dash-point is somewhat lower than the Mach limit, so the Mach limit is not encountered by the terminal transient maneuvers. Also, if the final altitude specified is greater than the terrain limit, then the terrain limit also may sometimes be eliminated from the problem. In this case the dynamic-pressure limit will be the only state constraint active.

Many methods have been devised for handling state-variable inequality constraints. Kelley [31], and Bryson and Denham [32], have used a penalty-function technique in which the constrained problem is converted to an unconstrained problem by adding a large quadratic penalty to the performance index whenever the constraint is violated. Jacobson and Lele [34], use a slack variable to convert the inequality constraint to an equality constraint, and then transform the problem to an unconstrained one of higher order. Constraints handled by penalty methods are termed "soft constraints" because it is not necessary that the constraints be satisfied precisely in order to generate a solution.

Problems formulated with "hard constraints" do require that the constraint be satisfied before a solution can be obtained. These methods require that the sequence of constrained and unconstrained arcs be known a priori. Bryson, Denham, and Dreyfus [37], and Bryson and Ho [24], develop a method in which the constraint, or one of its time derivatives, is adjoined to the Hamiltonian. Certain tangency conditions must be met at the entry to the constrained arc. The adjoint variables are discontinuous across the junctions and are non-unique along the constrained arc. Speyer and Bryson [4], present a variation of this method which utilizes the fact that the order of the system is reduced on the constrained portion of the trajectory. Here the adjoint variables are continuous across the junctions and unique along the constrained portion, but tangency

conditions must be satisfied at each junction point. As one would expect, each method carries with it its own advantages and disadvantages.

In the next chapter a detailed formulation of the terminal-transient problem is given. Results from a reduced-order "energy" model formulation of the problem are given in chapter three. In chapter four the point-mass model is developed, and the formulation of a direct adjoining method for enforcing the dynamic-pressure constraint in the optimal-control problem is presented along with numerical results to demonstrate the use of this method. Terminal transient results for the point-mass model formulation of the problem are discussed in chapter five.

2 Problem Statement

2.1 Equations of Motion

The equations of motion for the point-mass model of an aircraft can be written as

$$\dot{h} = V \sin \gamma \tag{2.1}$$

$$\dot{E} = \frac{V}{W}(\eta T - D) \tag{2.2}$$

$$\dot{\gamma} = \frac{g}{V}\left(\frac{L}{W} \cos \varphi - \cos \gamma\right) \tag{2.3}$$

$$\dot{X} = V \cos \gamma \cos \chi \tag{2.4}$$

$$\dot{Y} = V \cos \gamma \sin \chi \tag{2.5}$$

$$\dot{\chi} = \frac{g}{V}\left(\frac{L \sin \varphi}{W \cos \varphi}\right) \tag{2.6}$$

$$\dot{W}_f = \eta Q_f \tag{2.7}$$

where

$$V \equiv \sqrt{2g(E - h)}$$

and should be considered merely as an abreviated notation in the above equations. These equations embody the assumptions of thrust along the path, flight over a flat earth, and no winds. The selection of specific energy as a state variable rather than velocity is to obtain a better time scale separation. It is more slowly varying than either velocity or altitude [9]. This will be important when we consider the reduced-order "energy" model. The use of energy as a state variable in the point-mass model will also provide some convenience when comparing point-mass and energy-model solutions.

2.2 Symmetric Flight

In this study we will consider only the case of flight in the vertical plane. The heading angle χ and the bank angle φ are therefore fixed at zero in the dynamic equations. The fuel-flow-rate equation is also eliminated from the system equations since we will not be concerned with fuel expenditure. The vehicle weight will be considered to be constant.

The equations of motion are given as

$$\dot{h} = V \sin\gamma \tag{2.8}$$

$$\dot{E} = \frac{V}{W}(\eta T - D) \tag{2.9}$$

$$\dot{\gamma} = \frac{g}{V}(N - \cos\gamma) \tag{2.10}$$

$$\dot{X} = V\cos\gamma. \tag{2.11}$$

The control variables in this model are the load factor $N = \frac{L}{W}$ and the throttle control setting η, where $0 \leq \eta \leq 1$.

The load factor is subject to the limits

$$N \leq Q\frac{S_r}{W}C_{Lmax} \quad \text{(lift − coefficient limit)} \tag{2.12}$$

$$N \leq N_{max} \quad \text{(structural limit)} \tag{2.13}$$

while the following constraints apply to the state variables

$$h \geq h_T \quad \text{(terrain limit)} \tag{2.14}$$

$$\rho g(E - h) \leq \overline{Q} \quad \text{(dynamic pressure limit)} \tag{2.15}$$

$$M \leq \overline{M} \quad \text{(Mach limit)} \tag{2.16}$$

2.3 Modeling of the Aircraft Data

The drag coefficient is modeled as a parabolic function of the lift coefficient,

$$C_D = C_{D_o} + C_{Di}C_L^2 \ .$$

The zero-lift drag coefficient, C_{D_0}, and the induced drag coefficient, C_{D_i}, are functions of Mach number, and the maximum thrust is a function of both Mach number and altitude.

$$C_{D_o} = C_{D_o}(M)$$

$$C_{Di} = C_{Di}(M)$$

$$T = T(M,h)$$

The aircraft data used in the numerical computations are that of a high-performance fighter. The aircraft and atmospheric data are represented by cubic splines and spline lattices.[11,36] This method of representation provides a smooth curve-fit of the data. The thrust data used are for full throttle afterburning thrust.

2.4 The Terminal Transient

There are two basic ways in which a trajectory can lead from the dash point to a final state having a lower altitude and velocity than that of the dash point.[22] One is to decrease velocity and altitude simultaneously so that the velocity never exceeds the dash value. The other means is to allow the velocity to increase initially by rapidly decreasing altitude, and then decrease the velocity to the final value desired. Since the objective is to maximize the range covered, it appears that the optimal trajectory should spend as much time as possible at or above the dash velocity and as little time as possible at velocities below the dash velocity. It appears then that the minimum-time trajectory should begin with a dive from the dash point that increases the velocity while the altitude is decreased. This portion of the trajectory would be outside of the flight envelope where

the drag exceeds the thrust. When the drag causes the velocity to decrease to a value near that of the dash velocity, then it is appropriate to slow down as quickly as possible in order to meet the terminal state specification. To accomplish this, the throttle should be closed and the drag should be increased as much as possible by opening drag brakes and, theoretically, performing chattering between C_L bounds. These chattering maneuvers will be discussed in the next section.

In order to maximize the range covered, this throttle switching should occur at a point where the range rate is approximately equal to the value of the range rate at the dash point. A more precise statement can be made for energy-modelled flight, as will be seen. In other words, as much time as possible should be spent operating at $\dot{X}$ values that are greater than or equal to the value of $\dot{X}$ at the dash point. The range rate at the dash point is, from equation (2.11),

$$\dot{X}_d = V_d \ , \tag{2.17}$$

since the flight path angle is zero at the dash point. At the time the throttle is switched off, the range rate is

$$\dot{X}_s = V_s \cos \gamma_s \ , \tag{2.18}$$

where the path angle at the throttle switch time γ_s is not necessarily zero. Since the throttle switch should occur where $\dot{X}_d = \dot{X}_s$,then, upon equating (2.12) and (2.13),

$$V_d = V_s \cos \gamma_s \ , \tag{2.19}$$

or rewriting,

$$V_s = \frac{V_d}{\cos \gamma_s} \ . \tag{2.20}$$

Since $\cos\gamma_s$ is always ≤ 1, then $V_s \geq V_d$. This shows that the throttle-switch should occur at a velocity equal to or slightly above the dash velocity, depending on the value of γ_s . This throttle switching behavior will be investigated in the computational work presented in the following chapters.

2.5 Chattering Maneuvers

After the throttle is switched off the optimal maneuver possibilities become more complex. In order to insure that an optimal control exists, the hodograph figure must be convex.[2,26,33,38] The hodograph figure is the envelope of curves traced out in the state-rate space by varying the controls over their entire range at fixed values of the state-variables. The boundary of the figure defines an envelope of feasible operating points. For the symmetric-flight point-mass model, equations (2.9) and (2.10) are the only state-rate equations that depend explicitly on the control variables. In this case, only the $\dot{E} - \dot{\gamma}$ space need be considered.

The hodograph figure for the point-mass model of the present problem is shown in figure 9. If the hodograph figure were convex, the optimal control would lie on the boundary of the figure. As shown in the figure, the portion of the hodograph corresponding to zero-throttle operation is not convex. It is appropriate to consider a related problem with a hodograph figure which is the convex hull of the original, introducing additional controls as necessary. Thus a "relaxed" variational problem is formulated. One then approximates the solution of the relaxed problem by switching the controsl between points in hodograph space with a dwell time, vanishing in the limit, that will produce the desired control combination[2,38]. This is a so-called "chattering control". In figure 9, for zero-throttle operation, the control would switch operation

between points A and B, which is actually a switching between the upper and lower lift coefficient limits. The extreme lift coefficient values generate a large induced drag that maximize the rate at which the aircraft loses energy. In other words, simply switching the throttle off will not produce the largest possible rate of energy decrease. However, switching the throttle off and increasing the drag as much as possible will.

Chattering control is achieved analytically by introducing new control variables that encompass this characteristic. In order to avoid complication, chattering control is not implemented in the present study. For this reason, determining portions of optimal trajectories that lie beyond the throttle switching point is not possible with the present model. Therefore, the present analysis will only be concerned with trajectories that terminate at or before the throttle-switching time.

3 Energy-Model Analysis

3.1 Reduced-Order Modeling

Before attempting to analyze the point-mass model of the problem, it will be helpful to perform an analysis using a simpler, reduced-order model. The reduced-order results will provide a frame of reference for the point-mass modelled analysis. A detailed study of terminal-transient maneuvers using an energy-model approximation is presented in ref[35]. Reduced-order "energy" modeling is attractive for simplified computations while an approximation is obtained that compares at least qualitatively with the higher-order dynamic models.[3] Figure 2 shows energy and point-mass solutions from low altitude to the dash point for the aircraft model used in this study. It can be seen that the solutions agree closely in the supersonic region.

The specific energy, (originally " energy-height", ref[1]), is defined as the altitude at which the potential energy of the aircraft would be the same as the sum of its potential and kinetic energies at its present state. In the energy approximation, the potential and kinetic energies are assumed to be easily and rapidly interchangeable. The altitude,

velocity, and path angle can be varied more rapidly than the energy.[9] These approximations allow the formulation of the reduced-order "energy" model.

3.2 Formulation

Following the procedure of ref.[9], an interpolation parameter ε is introduced. Rewriting the dynamic equations (2.8) thru (2.11) with the parameter ε,

$$\varepsilon\dot{h} = V \sin\gamma \tag{3.1}$$

$$\dot{E} = \frac{V}{W}(\eta T - D) \tag{3.2}$$

$$\varepsilon\dot{\gamma} = \frac{g}{V}(N - \cos\gamma) \tag{3.3}$$

$$\dot{X} = V \cos\gamma \ . \tag{3.4}$$

The dynamic equations are now divided into two systems. For $\varepsilon = 1$, the original solution is obtained, while for $\varepsilon = 0$ the energy state model is found. In addition to reducing the order of the dynamical system, the energy modelling also makes the conditioning of the differential equations better than that of the complete Euler system.[9] This will allow longer integration time intervals than those possible with the complete state-Euler system.

Introducing $\varepsilon = 0$ into (3.1) and (3.3) implies that $\gamma = 0$ and $N = 1$, or, equivalently, $L = W$. Therefore the lift coefficient must be chosen so that lift is equal to the weight. The "fast" varying parameter h takes on the rôle of a control variable.[39]

The dynamical equations for the energy model are now

$$\dot{E} = \frac{V}{W}(\eta T - D) \tag{3.5}$$

$$\dot{X} = V \ . \tag{3.6}$$

Applying the maximum principle [14,15], the Hamiltonian for the system can be written for the minimum-time optimal control problem.

$$H = \lambda_E \frac{V}{W}(\eta T - D) + \lambda_x V + 1 \tag{3.7}$$

The resulting Euler equations are

$$\dot{\lambda}_E = -\frac{\partial H}{\partial E} \tag{3.8}$$

$$\dot{\lambda}_x = -\frac{\partial H}{\partial X} \ . \tag{3.9}$$

Since X does not appear in the Hamiltonian, λ_x will be a constant. The solution of this system requires that for a given energy, the altitude must be chosen so as to minimize the Hamiltonian.

Since the throttle control, η, appears linearly in the Hamiltonian, η is governed by a switching function $\frac{\partial H}{\partial \eta} = \lambda_E\left[\frac{VT}{W}\right]$. Since the term in the brackets is always positive, the switching function reduces to λ_E. In order to minimize the Hamiltonian, the control takes on the values

$$\eta = 0 \ \text{ if } \ \lambda_E > 0$$

$$\eta = 1 \ \text{ if } \ \lambda_E < 0 \ .$$

If λ_E becomes identically zero for some non-zero time interval then an intermediate-throttle ("singular") arc arises.

The multipliers λ_E and λ_x can be thought of as "weighting" parameters. The magnitude of a multiplier determines the relative importance or "weight" placed on the corresponding state variable. The value of h chosen to minimize the Hamiltonian at a given energy will thus depend on the magnitudes of the multipliers λ_E and λ_x. Also, the value of the Hamiltonian is zero. It is required that the Hamiltonian be constant since the independent variable, time, does not appear explicitly in the right-hand sides of the differential equations. Only the ratio of the two multipliers is important in this model and not their actual values.

Let R denote the ratio of the multipliers,

$$R = \frac{\lambda_x}{\lambda_E} .$$

An initial-value problem can be formulated to solve the system of equations for various values of R. The algorithm of ref[39] is used here to perform the numerical calculations. The control inequality constraints are handled by the technique of Valentine.[39,9] The Hamiltonian is augmented by adjoining to it the constraints (2.12) through (2.16) with multipliers λ_i , i = 1,...,5,

$$\bar{H} = H + \sum_{i=1}^{5} \lambda_i \beta_i$$

where β_i represents the constraint. If a particular constraint is not active, the corresponding multiplier is zero. If the constraint is active, then the multiplier is calculated from the optimality condition

$$\frac{\partial \bar{H}}{\partial h} = 0 \ .$$

3.3 Numerical Computations

If the range multiplier λ_x is set to zero and λ_E is a large positive value, the resulting trajectory will lead to the high-energy point on the level flight envelope. This solution, called the energy climb, is shown in figure 3 for the aircraft of this study. As the initial value of R is increased, i.e., λ_x is increased relative to λ_E, the resulting solution leads to points on the flight envelope that are lower in energy. When a certain initial value of R is reached the solution will fair into the high velocity point on the flight envelope. Let R_d denote this value of R. This trajectory will be the range optimal solution and is shown in figure 4.

If the integration of the system is allowed to proceed for a period of time that is greater than that needed to reach the dash point, an interesting behavior is observed. For initial values of R that are slightly smaller than R_d, the trajectory leads to the dash point and then curves upward and approaches the high energy point on the flight envelope, as shown in figure 5. For initial values of R that are slightly greater than R_d, the resulting solution fairs downward from the dash point to a lower energy level. This portion of the trajectory from the dash point to a lower energy and altitude is the terminal transient of interest in the present study.

A solution containing this terminal-transient maneuver is shown in figure 6. The terminal maneuver begins with a dive that increases the velocity and rapidly decreases the altitude until the dynamic pressure constraint is encountered. It then rides the

dynamic-pressure inequality constraint as the velocity decreases until the terminal flight time is reached.

The velocity as a function of time is shown in figure 7. The dash velocity value is reached at approximately 530 seconds. The velocity then climbs to some maximum value, after which it decreases, returning to a value equal to that of the dash velocity at a time of 735 seconds. The corresponding time-history of the throttle switching function, λ_E, is shown in figure 8. It can be seen that λ_E changes from negative to positive at a time of 735 seconds.

Figures 7 and 8 show that the throttle-switching time occurs at the same time that the velocity decreases to the dash speed. Since $\gamma = 0$ in the energy model solution, it follows from (2.20) that this should be the case. Therefore, as expected, the time history of the throttle switching function is such that the throttle switch would occur at the time that the velocity is equal to the dash value.

In ref [22], this terminal transient dive for the energy-model solution is described as an instantaneous dive that takes place at a constant energy level. Because altitude is a control variable in the energy-model formulation, it can be discontinous. If at a given energy value there exist two values of altitude that produce the same minimum value of the Hamiltonian, a discontinuity will occur in the altitude time-history at that energy level. This would appear in the altitude-velocity space as an instantaneous dive at constant energy.

The hodograph figure for the energy model formulation is shown in figure 22. The line tangent to the hodograph in the figure is the constant Hamiltonian value at the dash point. In order for a minimum to exist at two points, this constant Hamiltonian line must be tangent to the hodograph figure at two points. In other words, the hodograph figure could not be convex for the full-throttle operation.

As the figure illustrates, this full-throttle portion of the hodograph is convex and therefore, two minima would not exist. For this reason, the dive does not occur as a constant energy discontinuity in altitude.

As the diving maneuver progresses from the dash point, the constant Hamiltonian lines become more nearly horizontal and the point of tangency may approach point A in the figure. Should λ_E become zero, the constant Hamiltonian line becomes horizontal and the operating point shifts from point A to point B, which lies on the zero-throttle portion of the hodograph. This switch from point A to point B corresponds to the throttle switch that occurs when $\lambda_E = 0$.

Just as in the point-mass case, the zero-throttle portion of the hodograph figure is not convex. High-drag maneuvers would be required here for zero-throttle operation.

4 Point-Mass Model with State Constraints

4.1 Formulation

The energy-model solution of the previous chapter provides some insight into the behavior of the terminal-transient maneuver. In this chapter, the more complex point-mass model of the aircraft will be developed and the method for handling the dynamic-pressure constraint presented.

The equations of motion describing the point-mass model of an aircraft under the assumptions outlined in chapter two are given by equations (2.8) through (2.11) and are repeated here for convenience.

$$\dot{h} = V \sin \gamma \tag{4.1}$$

$$\dot{E} = \frac{V}{W}(\eta T - D) \tag{4.2}$$

$$\dot{\gamma} = \frac{g}{V}(N - \cos \gamma) \tag{4.3}$$

$$\dot{X} = V \cos \gamma \tag{4.4}$$

Applying the maximum principle [14,15], the Hamiltonian for the point-mass system is

$$H = \lambda_h V \sin \gamma + \lambda_E \frac{V}{W}(\eta T - D) + \lambda_\gamma \frac{g}{V}(N - \cos \gamma) + \lambda_x V \cos \gamma \tag{4.5}$$

and the resulting Euler equations are given by

$$\dot{\lambda}_h = -\frac{\partial H}{\partial h} \tag{4.6}$$

$$\dot{\lambda}_E = -\frac{\partial H}{\partial E} \tag{4.7}$$

$$\dot{\lambda}_\gamma = -\frac{\partial H}{\partial \gamma} \tag{4.8}$$

$$\dot{\lambda}_x = -\frac{\partial H}{\partial X} \ . \tag{4.9}$$

The throttle-control logic obtained from $\frac{\partial H}{\partial \eta}$ is the same as in the energy model formulation of chapter three,

$$\eta = 0 \text{ if } \lambda_E > 0$$

$$\eta = 1 \text{ if } \lambda_E < 0$$

$$0 \leq \eta \leq 1 \text{ if } \lambda_E = 0 \ .$$

The optimal load factor is obtained from $\frac{\partial H}{\partial N} = 0$. This gives the expression for the load factor as,

$$N = \frac{\lambda_\gamma g Q S_r}{2\lambda_E V^2 C_{Di} W} . \tag{4.10}$$

4.2 Dynamic Pressure Constraint

The dynamic pressures that occur in the terminal transient trajectory will tend to exceed the maximum allowable dynamic pressure. For this reason, a constraint must be introduced to insure that the dynamic-pressure limit will not be exceeded. In the present work, the direct adjoining method given in refs.[24,37] will be used to treat the state constraint. In this method the Hamiltonian is augmented along the constrained arc by adjoining to it the constraint or an appropriate time derivative of the constraint. Certain conditions must be satisfied at the junctions between constrained and unconstrained arcs. As a result, a multi-point boundary value problem is obtained which will be solved computationally using an existing algorithm designed for the solution of such problems.

The dynamic-pressure constraint can be written in terms of the state variables as

$$S = \rho g(E - h) - \overline{Q} \leq 0. \tag{4.11}$$

Notice that this expression does not contain the control variable N. The first time derivative of (4.11) does contain the control variable however, therefore, (4.11) is a first order constraint. The first time derivative of the constraint is

$$\dot{S} = g\frac{\partial \rho}{\partial h}\dot{h}(E - h) + \rho g(\dot{E} - \dot{h}) . \tag{4.12}$$

The load factor N appears in (4.12) through the substitution from (4.2). Since the constraint (4.11) must vanish along the constrained arc, its time derivative must also be zero. For this reason the constraint (4.11) can be imposed by requiring that the time derivative be zero along the constrained arc and that, at the time the constrained arc is encountered, (4.11) is identically zero. Equation (4.12) can now be considered to have replaced the state constraint, and (4.11) becomes the "tangency condition" that must be satisfied at the entry time to the constrained arc.

Following the procedure of ref.[24], the Hamiltonian is augmented by adjoining (4.12) to it with a multiplier μ.

$$\bar{H} = H + \mu\dot{S}\,, \tag{4.13}$$

where H is given by (4.5). Since the optimality conditions now require that $\frac{\partial \bar{H}}{\partial N} = 0$, this yields an expression that can be used to solve for the multiplier μ. Another relationship is needed in order to solve for the control variable N. Since N appears in the equation $\dot{S} = 0$, this equation can be solved for the load factor. Since $\dot{S} = \dot{Q}$, the control obtained is simply the value needed to insure that the trajectory remains on the constraint.

The following conditions apply to μ,

$$\mu = 0 \text{ if } S < 0 \tag{4.14}$$

$$\mu > 0 \text{ if } S = 0 \tag{4.15}$$

where S is the constraint (4.11). In addition, μ must be monotonically non-increasing along the constrained arc.[42,43] Therefore,

$$\dot{\mu} \leq 0 \text{ if } S = 0\ . \tag{4.16}$$

The costate variables will experience discontinuities across the junctions between constrained and unconstrained arcs. In ref [37], it is pointed out that these discontinuities are not unique. The requirements can be satisfied entirely at the entry time to the constrained arc, entirely at the exit time, or, partially at both junction points. In the present formulation, the entry time t_1 is the point chosen to satisfy the discontinuities. Letting t_1^- be the time an instant before the constrained arc is encountered and t_1^+ the time just after the contact time, the jumps are given by

$$\lambda^T(t_1^-) = \lambda^T(t_1^+) + \pi^T \frac{\partial C}{\partial x(t_1)} \tag{4.17}$$

where x denotes the array of state variables, λ^T the costates, and π^T is an array of "jump" multipliers. C is the vector of "tangency" conditions that must be satisfied at t_1.[24] Since the state variables γ and X do not appear in the constraint S, λ_γ and λ_x are continuous across t_1.

Because the constraint is first-order in the present case, there is only one "tangency" condition, which is simply the constraint (4.11). For this reason π and C in (4.17) are scalars here. It can be shown that at t_1^+ the multiplier π is equal to the value of the constraint multiplier $\mu(t_1^+)$ and therefore, π must also be positive.(see appendix A)

The multiplier μ will be the parameter that signals when the trajectory should leave the constrained arc. When μ goes to zero the trajectory should leave the arc, so $\mu(t_2) = 0$ becomes an internal boundary condition. This condition is also needed to insure that a unique solution exists. The time history of μ along the constraint is dependent on the magnitude of the jump in the adjoints. By specifying that μ be zero at the exit time, the jump in the adjoints will have to be such that this condition is satisfied. This condition is also necessary in order to insure that the adjoint variables are continuous across the exit time.

There is also the possibility that the Hamiltonian can be discontinuous at t_1,

$$H(t_1^-) = H(t_1^+) - \pi\frac{\partial S}{\partial t_1} , \tag{4.18}$$

but since S does not depend explicitly on time in the present case, the Hamiltonian will be continuous across the junction.

$$H(t_1^-) = H(t_1^+) \tag{4.19}$$

Using (4.19) it can be shown that the load factor is also continuous across t_1.(see appendix B)

The throttle control for the constrained problem is obtained from $\frac{\partial \bar{H}}{\partial \eta} = 0$. Since η appears linearly in (4.12), the throttle control will move according to a switching function different from that of the unconstrained problem. The throttle switching function becomes λ_γ instead of λ_E.(see appendix C) The throttle switching to minimize the augmented Hamiltonian will be such that

$$\eta = 1 \text{ if } \lambda_\gamma < 0$$

$$\eta = 0 \text{ if } \lambda_\gamma > 0$$

$$0 \leq \eta \leq 1 \text{ if } \lambda_\gamma = 0 .$$

4.3 Numerical Example

Before attempting to analyze the terminal transient behavior, it will be instructive to work a simpler example to demonstrate the state-constraint formulation outlined above.

This will provide a comparison between the constrained and unconstrained trajectories and allow an analysis of the parameters associated with this direct-adjoining approach of handling the constraint.

In order to generate a test problem that is uncomplicated by throttle-switching behavior, the dynamic pressure limit is moved well inside the flight envelope. A minimum-time trajectory between two points inside the flight envelope is generated that would violate this constraint if it were absent. The problem is then solved with the constraint instated. Figure 10 shows the constraint along with the constrained and unconstrained solutions. As one would expect, the unconstrained trajectory connects the two endpoints in a shorter time than the constrained path.

Figure 11 shows the time-history of the multiplier μ along the constrained arc. In accordance with (4.15), μ remains positive throughout the constrained arc. Also, it can be seen that μ is always decreasing. This behavior agrees with (4.16). The initial value of μ on the constraint is equal to the value of the constant multiplier π and it decreases to zero at the exit time of the constrained arc.

Figure 12 shows the time-histories of the adjoint variables λ_E and λ_h throughout the entire trajectory. These two variables experience a jump at the entry time to the constrained arc, but they are continuous at the exit time.

This test example has demonstrated the behavior of the parameters associated with the method used here for handling the constraint, and has shown that they behave in accordance with the conditions outlined in the previous section. This direct-adjoining method will be used to treat the dynamic-pressure constraint during the analysis of terminal transient maneuvers in the next chapter.

5 Solutions with the Point-Mass Model

5.1 Results

The point-mass formulation presented in the preceding chapter will now be used to analyze the terminal transient maneuvers. As mentioned earlier, the entire minimum-time mission can be divided into three segments. For this reason, the terminal portion can be isolated from the climb and dash segments. Trajectories can be generated that originate at the dash point and proceed forward in time until the final state is reached, rather than integrating over the entire flight time from the low-altitude starting point. This scheme will be used here in order to reduce the computational expense and reduce the possibilities of error growth that may occur with the long integration times.

The minimum-time trajectory to the dash point for the point-mass model formulation is shown in figure 2. In figure 13, two terminal trajectories are shown that were generated without the constraint enforced and with the throttle-control variable η fixed at $\eta = 1$. The vertical line on the figure depicts the dash velocity. Recall from equation (2.20) that the throttle switch should occur at a velocity slightly above the dash velocity. One of the

two trajectories in figure 13 terminates just before the dash velocity and therefore, very near the throttle switching time. The other solution however, continues beyond the throttle switching point and cannot be considered an optimal solution because of frozen throttle and unrelaxed drag modelling. In figure 14, the constrained solution to this same final state is shown. The trajectory contacts the constraint, rides it for some time, and then leaves the constrained arc in order to meet the final-state specification. The discontinuities in the adjoints and the behavior of the constraint multiplier μ are similar to the behavior found in the example presented in the previous chapter. As one would expect, the unconstrained version takes less time than the constrained version to reach the final state.

Attention should be focused on trajectories that terminate at the throttle-switching time in order to accomodate the shortcomings of the unrelaxed model. Figure 15 shows a constrained solution that terminates on the constraint near the point where the throttle switch should occur. It will be of interest to investigate the behavior of the throttle-switching function for this solution. Figure 16 shows a plot of the range rate and the path-angle multiplier as the throttle-switching time is approached. At the point where λ_γ is zero, the range rate should be equal to the dash velocity, since λ_γ is the throttle switching function in this case. The dash velocity is shown by the horizontal line on the figure. As illustrated in the figure, λ_γ becomes zero slightly before the range rate becomes equal to the dash value. The actual disagreement here is less than 1 $\frac{\text{ft.}}{\text{sec.}}$. This yields an error of approximately 0.03% when comparing the actual value of $\dot{X}$ here at the switching time to the dash velocity value that it should have at this point. This slight disagreement may be caused by the fact that the integration of the solution does not begin exactly at the dash point.

Integration from the exact dash point is not actually possible because the dash point is an equilibrium point. The equations of motion at the dash point are

$$\dot{h} = 0 \tag{5.1}$$

$$\dot{E} = 0 \tag{5.2}$$

$$\dot{\gamma} = 0 \tag{5.3}$$

$$\dot{X} = V_d \ . \tag{5.4}$$

If the integration started at this point, the only state variable that will change is the ignorable variable X. For this reason, it is necessary to start the integration procedure at a point slightly perturbed from the dash point. Even solutions with initial values that are extremely close to the dash point spend a large amount of the integration time in the vacinity of the dash point where the dynamics are very slow.

A plot of range rate vs. throttle switching function, similar to figure 16, is shown for an unconstrained trajectory in figure 17. Here the throttle switching function is λ_E . As expected, the range rate becomes equal to the dash velocity very near the point where λ_E is zero. The agreement between range rate and dash velocity values at $\lambda_E = 0$ is closer here than in the constrained solution of figure 16.

An interesting observation can be made concerning the throttle switching function for the unconstrained solutions. The load factor is computed from equation (4.10) as

$$N = \frac{\lambda_\gamma g Q S_r}{2\lambda_E V^2 C_{Di} W} \ . \tag{5.5}$$

When the throttle switching time is approached, λ_E approaches zero. Since λ_E appears in the denominator of (5.5), λ_γ must also approach zero in order to avoid an infinite load factor. (Notice that the remaining terms in the equation will not become zero.) Figure

18 illustrates the behavior of λ_E and λ_γ in the vacinity of the throttle switching time. As required, they both approach zero at very nearly the same time.

This coupling between λ_E and λ_γ need not hold for the constrained case. The equation for the load factor is obtained from $\dot{Q} = 0$, and is not a function of the multipliers. In fact, for the constrained case, λ_E and λ_γ should not go to zero simultaneously. The equation for the constraint multiplier μ is given by equation (A.1) as

$$\mu = \frac{\lambda_\gamma W}{2V^2 N \rho D_i} - \frac{\lambda_E}{\rho g} . \tag{5.6}$$

As pointed out in chapter four, μ must be positive along the constraint and become zero at the exit junction point. If λ_E becomes zero at the same time that λ_γ does, then μ would also be zero at this point. This would require that the throttle switching time coincide with the exit time of the constrained arc, which need not be the case. Also, by examining (5.6), one can see that λ_γ must change sign before λ_E does in order that μ remain positive along the constraint. This is because both of the multipliers are initially negative on the constraint and the remaining parameters in (5.6) remain positive. Figure 19 shows the time histories of λ_E and λ_γ along the constrained arc. The figure illustrates that λ_γ changes sign long before λ_E would. In fact, λ_E approaches zero very slowly, and appears to be almost constant in the figure. Because of the short duration of the constrained arcs generated here, λ_E does not even experience a sign change along the constrained portion.

It would be of interest to generate a solution that contacts the constraint, rides it for some time, and then, approaches a final point above the constraint that lies before the throttle switching time. A solution of this type would be similar to the solution shown in figure 15, except that the trajectory would be required to leave the constraint in order to meet the final state. Because of this, the constrained arc would become shorter than

that shown in the figure. If the constrained portion becomes too short, the solution may resemble a touch point rather than a constrained arc.

Finding numerical solutions to trajectories with very short constrained arcs can be difficult because the junction points are extremely close together. In the solution of figure 15, the constrained arc is only approximately two seconds in length. Requiring the solution to leave the constrained arc in order to meet a final state above the constraint will reduce the constrained portion to an even smaller time interval.

As a possible remedy to this problem, an attempt was made to find solutions that would violate the constraint more severely, and therefore, possibly allow for the generation of solutions with constrained arcs of a longer time interval before the throttle switching time is reached. By specifying the final value of the path angle to be some positive value, the resulting solutions tend to violate the constraint more severely, but an interesting phenomenon occurs.

It appears that a high specific energy is required in order to execute maneuvers to these final path-angle values. A family of these solutions for various final path-angle values is shown in figure 20. The trajectories spend some time in the initial stage approaching a higher energy level than that of the dash point. As the final path angle is increased, the energy level that the solution approaches before descending becomes greater. A large portion of the total flight time is spent in this energy-increasing climb. Constrained solutions for these final states could not be found. The decrease in altitude occurs very rapidly in this case. When the dynamic-pressure constraint is introduced into the problem, large load factors are required near the contact time of the constraint in order to insure that the constraint is not violated. The existence of solutions to these final state specifications in the presence of the constraint is questionable.

Finally, it will be interesting to see how an energy-model solution compares to a point-mass solution for a terminal trajectory between similar points. Figure 21 shows

two such trajectories. The initial point here is the equilibrium point that results from the energy-model analysis, and is determined by the scheme described in chapter three. This "dash point" found in the energy model approximation is slightly lower in altitude and velocity than the actual dash point. Because of this, the point-mass solution spends some time in the initial portion of the flight time increasing altitude and approaching a higher energy level. It then crosses the flight envelope at a point closer to the actual dash point and dives rapidly towards the dynamic pressure constraint.

The altitude and velocity time histories differ somewhat in the two solutions. The energy-model has the path-angle always zero, but the actual path-angle values that occur in the point-mass solution are not extremely close to zero. This zero path-angle modelling feature is probably the cause of some of the inconsistancies between the two solutions. Also, the energy-model solution takes less time to cover the specified range than the point-mass solution does. This would also be expected, due to the zero path-angle feature of the energy-model formulation.

6 Conclusions and Future Work

6.1 Discussion

The analysis presented in this work focuses on two major objectives. One is the formulation of optimal control problems with state constraints, and the other is the study of the terminal-transient maneuvers of the minimum-time dash mission.

The use of the direct-adjoining approach to enforce the dynamic-pressure limit proved to be successful in the test example of chapter four and during the analysis of the terminal transient maneuvers in the preceding chapter.

The energy model analysis has provided an approximation to the more complex point-mass model and has suggested behavior of the throttle switching function. The results determined that the dive experienced during the terminal maneuver does not occur as a constant energy discontinuity in altitude, as previously reported.[22]

The point-mass formulation of the problem has provided a detailed study of the terminal-transient maneuvers that terminate near the throttle switching point. The

appearance of different throttle switching functions for constrained and unconstrained solutions was determined.

6.2 Future Work

In the present effort, the analysis is restricted to trajectories that terminate near the throttle switching time, as discussed in chapter two. It would certainly be of interest to adapt the problem formulation to include relaxed drag and hence C_L chattering maneuvers in order to provide a convex hodograph figure and allow an in-depth study of trajectories that continue to final states well beyond the throttle-switching point.

Solutions of this type may simply ride the constraint until the final state is approached, or they may experience a sequence of constrained and unconstrained arcs. On the other hand, it may not even be possible to ride the constraint once the throttle has been switched off. Partial throttling may be required in order to produce a solution that remains on the constraint. Investigating these questions would be an interesting extension of the present work.

Appendix A: Constraint and Jump Multipliers

The equation for μ along the constrained arc is obtained from $\frac{\partial \tilde{H}}{\partial N} = 0$, where $\tilde{H}$ is given by (4.13), and is

$$\mu = \frac{\lambda_\gamma W}{2V^2 N \rho D_i} - \frac{\lambda_E}{\rho g} \ . \tag{A.1}$$

Letting + denote quantities an instant after the contact time of the constrained arc t_1, and - denote quantities an instant before t_1, (A.1) can be written as

$$\mu^+ = \frac{\lambda_\gamma W}{2V^2 N \rho D_i} - \frac{\lambda_E^+}{\rho g} \tag{A.2}$$

for t_1^+ since λ_E is the only quantity in (A.1) that experiences a discontinuity across t_1. (It is shown in appendix B that $N^+ = N^-$)

The jump in λ_E is given by (4.15) as

$$\lambda_E^+ = \lambda_E^- - \pi \rho g \tag{A.3}$$

Upon substituting (A.3) into (A.2)

$$\mu^{+} = \frac{\lambda_{\gamma} W}{2V^{2} N \rho D_{i}} - \frac{\lambda_{E}^{-}}{\rho g} + \pi \ . \tag{A.4}$$

The first two terms on the right-hand side of (A.4) represent the value of μ at t_I^-, or

$$\mu^{-} = \frac{\lambda_{\gamma} W}{2V^{2} N \rho D_{i}} - \frac{\lambda_{E}^{-}}{\rho g} \ . \tag{A.5}$$

Rewriting (A.4),

$$\mu^{+} = \mu^{-} + \pi \ .$$

The value of μ^- is zero by definition because at t_I^- the constraint is not yet active. Therefore,

$$\mu^{+} = \pi \ . \tag{A.6}$$

Appendix B: Continuity of Load Factor Across Contact Time

Since the contact time of the constrained arc t_1 does not appear in the constraint S in (4.16), the Hamiltonian will be constant across t_1.

$$H(t_1^-) = H(t_1^+) \tag{B.1}$$

Substituting (4.5), and (4.1) thru (4.4), (B.1) can be written as

$$\lambda_h^- V \sin\gamma + \lambda_E^-(T - D^-)\frac{V}{W} + \lambda_\gamma \frac{g}{V} N^- = \tag{B.2}$$

$$\lambda_h^+ V \sin\gamma + \lambda_E^+(T - D^+)\frac{V}{W} + \lambda_\gamma \frac{g}{V} N^+$$

since λ_x, λ_γ and the state variables are continuous across t_1. This equation also assumes that the throttle does not switch across t_1, and therefore, η remains equal to one.

Rearranging (B.2)

$$(\lambda_h^+ - \lambda_h^-)V \sin\gamma + (\lambda_E^+ - \lambda_E^-)\frac{V}{W}(T - D^+) \tag{B.3}$$

$$+ \lambda_\gamma \frac{g}{V}(N^+ - N^-) + \lambda_E^- \frac{V}{W}(T - D^+ - T + D^-) = 0$$

Substituting (4.15), (4.1) and (4.2), (B.3) becomes

$$- \pi\frac{\partial Q}{\partial h}\dot{h} - \pi\frac{\partial Q}{\partial E}\dot{E}^+ + \tag{B.4}$$

$$\lambda_\gamma \frac{g}{V}(N^+ - N^-) - \lambda_E \frac{V}{W}(D^+ - D^-) = 0 \ .$$

The first two terms in (B.4) can be written as $-\pi\dot{Q}^+$ and are zero because $\dot{Q}^+$ is zero. With this in mind, and noting that $D = D_o + N^2 D_i$, (B.4) now reduces to

$$\lambda_\gamma \frac{g}{V}(N^+ - N^-) - \frac{\lambda_E^- V D_i}{W}(N^{+2} - N^{-2}) = 0 \ . \tag{B.5}$$

which can be rewritten as

$$(N^+ - N^-)[\lambda_\gamma \frac{g}{V} - \frac{\lambda_E^- V D_i}{W}(N^+ - N^-)] = 0 \ . \tag{B.6}$$

Now, from the condition $\frac{\partial H^-}{\partial N^-} = 0$, an expression for N^- is obtained

$$N^- = \frac{\lambda_\gamma g W}{2\lambda_E^- V^2 D_i} \ , \tag{B.7}$$

or, upon rearranging

$$\lambda_\gamma \frac{g}{V} = \frac{2N^- \lambda_E^- V D_i}{W} \ . \tag{B.8}$$

Substituting (B.8) into (B.6) and simplifying,

$$(N^+ - N^-)[\frac{\lambda_E^- VD_i}{W}(2N^- - N^+ - N^-)] = 0 \ , \tag{B.9}$$

or, rearranging

$$-\frac{\lambda_E^- VD_i}{W}(N^+ - N^-)^2 = 0 \ . \tag{B.10}$$

From (B.10) it follows that $N^+ = N^-$ exept for the singular case $\lambda_E^- = 0$. Therefore, the control is continuous across the junction of the constrained and unconstrained arcs, provided that $\lambda_E \neq 0$.

Appendix C: Throttle Switching Function On The Constraint

The throttle switching function along the constrained arc is obtained from $\frac{\partial \bar{H}}{\partial \eta} = 0$, where $\bar{H}$ is given by (4.13). Letting swt denote the switching function,

$$swt = \frac{TV}{W}(\lambda_E + \mu\rho g) \ . \tag{C.1}$$

Substituting equation (A.1) for μ along the constraint, (C.1) can be written as

$$swt = \frac{Tg}{2VD_i}\left[\frac{\lambda_\gamma}{N}\right] \ . \tag{C.2}$$

Since only the sign of the switching function is important and not its magnitude, the quantity outside the brackets in (C.2) can be neglected because it is always positive. The switching function then reduces to

$$swt = \frac{\lambda_\gamma}{N} \ . \tag{C.3}$$

If it is assumed that the load factor remains positive along the constrained arc, as it is for the present work, the switching function simply becomes

$$\text{swt} = \lambda_{\gamma} \ . \tag{C.4}$$

References.

1. Merritt, S.R., Cliff, E.M. and Kelley, H.J., "Energy-Modelled Climb and Climb-Dash - The Kaiser Technique", *Automatica*, Vol.21, May, 1985, pp. 319-321.

2. Kelley, H.J., and Sullivan, H.C.,"Roll Modulated Lifting Entry Optimization", *AIAA Journal*,Vol.11,No.7, July 1973 pp 913-915.

3. Bryson, A.E., Desai, M.N. and Hoffman, K., "Energy-State Approximation in Performance Optimization of Supersonic Aircraft", *Journal of Aircraft*, Vol.6, November 1969, pp.481-488.

4. Speyer, J.L. and Bryson, A.E., "Optimal Programming Problems With a Bounded State Space ", Joint Automatic Control Conference, (JACC), pp 485-491, 1968. Vol. 9, February 1972, pp.108-114.

5. Kelley, H.J. and Lefton, L., "Supersonic Aircraft Energy Turns", *Automatica*, Vol.8, September 1972, pp.575-580.

6. Wasow, W., "Asymptotic Expansions for Ordinary Differential Equations", John Wiley and Sons, New York, 1975.

7. Kelley, H.J. and Edelbaum, T.N., "Energy Climbs, Energy Turns and Asymptotic Expansions", *Journal of Aircraft*, Vol.7, January 1970, pp.93-95.

8. Kelley, H.J., "Flight-Path Optimization with Multiple Time Scales", *Journal of Aircraft*, Vol.8, April 1971, pp.238-240.

9. Kelley, H. J., "Aircraft Maneuver Optimization by Reduced-Order Approximation", *Control and Dynamic Systems*, Vol. 10, edited by C. T. Leondes, Academic Press, New York, 1973, pp.131-178.

10. Etkin, B.,"Dynamics of Atmospheric Flight", John Wiley and Sons, New York, 1972.

11. Gerald, C.F., Wheatley, P.O.,"Applied Numerical Analysis", Addison-Wesley Publishing Co., Reading, Mass., 1985.

12. Falco, M., and Kelley, H.J.,"Aircraft Symmetric Flight Optimization", *Control and Dynamic Systems*, Vol.10, Academic Press, New York, 1973.

13. Keller, H.B.,"Numerical Solution of Two Point Boundary Value Problems", J.W. Arrowsmith Ltd., Bristol 3, England, 1976.

14. Pontryagin, L.S., Boltyanskii, V.G., Gamkrelidze, R.V., Mishchenko, E.F.,"The Mathematical Theory of Optimal Processes", John Wiley & Sons, New York, 1962.

15. Leitmann, G.,"An Introduction to Optimal Control", McGraw-Hill, New York, 1966.

16. Kelley, H.J., Uzzell, B.R., and McKay, S.S., "Rocket Trajectory Optimization by a Second-Order Numerical Technique", *AIAA Journal*, Vol.7, No.5, May 1969, pp. 879-885.

17. Leitmann, G.,"Optimization Techniques", Academic Press, New York, 1962.

18. Weston, A. R., Cliff, E. M. and Kelley, H. J., "Altitude Transitions in Energy Climbs", *Automatica*, Vol. 19, No. 2, 1983, pp.199-202.

19. Menon,P.K.A.,"Optimal Symmetric Flight With an Intermediate Vehicle Model", *Journal of Guidance, Control, and Dynamics*, Vol.8, May 1985, pp.312-319.

20. Denn, M.M.,"Optimization by Variational Methods", R.E.Kreiger, New York, 1978.

21. Weston, A.R., Cliff, G. and Kelley, H., "On-Board Near-Optimal Climb-Dash Energy Management", *Journal of Guidance and Control*, Vol.8, No.3, 1985, pp.320-324.

22. Weston, A.R., "On-Board Near-Optimal Climb-Dash Energy Management", Ph.D. dissertation, Department of Aerospace and Ocean Engineering, VPI&SU, 1982

23. Vinh, N.X., "Optimal Trajectories in Atmospheric Flight", Elsevier, Amsterdam, 1981

24. Bryson, A.E. and Ho, Y.-C., "Applied Optimal Control", Hemisphere, Washington, 1975

25. Kelley, H.J., Cliff, E.M., Weston, A.R., "Energy-State Revisited", *Optimal Control Applications and Methods*, Vol.7, 1986, pp.195-200.

26. Houlihan, S.C.,Cliff, E.M.,Kelley, H.J.,"A Study of Chattering Cruise",*Journal of Aircraft*, Vol.19, Feb.1982, pp.119-124.

27. Miele, A.,"Flight Mechanics", Addison-Wesley, Reading, MA., 1962.

28. Bliss, G.A.,"Calculus of Variations", The Open Court Publishing Co., LaSalle, Il.,1925.

29. Visser, H.G.,"Energy Management of Three-Dimensional Minimum-Time Intercept",*Journal of Guidance, Control and Dynamics*, to appear.

30. Houlihan, S.C.,"Fuel Optimization of Aircraft Cruise Using Chattering Control", M.S.Thesis, Department of Aerospace and Ocean Engineering, VPI&SU, 1980.

31. Kelley, H.J.,"Method of Gradients", Chapter 6 of *Optimization Techniques* (G. Leitmann, ed), Academic Press, New York, 1962.

32. Bryson, A.E.,and Denham, W."Optimal Programming with Inequality Constraints II; Solution By Steepest Ascent", *AIAA Journal 2*, 25-34, 1964.

33. Kelley, H.J., Shinar, J., and Bar-Moshe, D.," Variable Sweep Optimization", *Automatica*, Vol.15, pp 403-409, 1979.

34. Jacobson, D.H., and Lele, M.M.,"A Transformation Technique for Optimal Control Problems With A State Variable Inequality Constraint", *IEEE Trans. Aut. Control*, AC-14, 457-464, 1969.

35. Lemercier, C.A.,"Terminal Transient for Optimal Dash", VPI&SU report fulfilling ENSAE requirements for the degree of Engineer, June 1986.

36. Shinar, J., Merari, A., Blank, D., and, Medinah, E.M.," Analysis of Optimal Turning Maneuvers in the Vertical Plane", *Journal of Guidance and Control*, Vol.3, pp. 78-85, 1980.

37. Bryson, A.E., Denham, W.F., and Dreyfus, S.E.,"Optimal Programming Problems With Inequality Constraints I.: Necessary Conditions For Extremal Solutions",*AIAA Journal 1*, 1963, pp.2544-2550.

38. Cliff, E.M., Kelley, H.J., and Lefton, L.,"Thrust-Vectored Energy Turns", *Automatica*,Vol.18, No.5, pp 559-564,1982.

39. Lefton, L.,and, Krenkel, R.,"A User's Guide to the Supersonic Energy Turns Computer Program", Analytical Mechanics Associates ,Inc., Report No.72-12 August 1972, Revised February 1975.

40. Erzberger, H. and Lee, H.,"Constrained Optimum Trajectories with Specified Range", *Journal of Guidance and Control*,Vol.3, Jan-Feb 1980, pp.78-85.

41. Jacobson, D.H., Lele, M.M., and Speyer, J.L.,"New Necessary Conditions of Optimality for Control Problems with State-Variable Inequality Constraints", *J. Math. Anal. Appl. 35*,1971, pp.255-284.

42. Kreindler, E.,"Additional Necessary Conditions for Optimal Control with State-Variable Inequality Constraints", *J. Optimization Theory Appl. 38* , 1982, pp.241-250.

43. McIntyre, J. and Paiewonsky, B.,"On Optimal Control with Bounded State Variables",in; Leondes,C.T.(ed.), Advances in Control Systems 5, Academic Press,New York, 1967.

44. Hartl, R.,"A Survey of the Optimality Conditions for Optimal Control Problems With State Variable Inquality Constraints", Operational Research 84, Elsevier Science Publishers,1984.

45. Vlassenbroeck, J.,"An algorithm for Optimal Control Problems With State Inequality Constraints",Dept. of Analytical Mechanics, Vrije Universiteit Brussel,Brussels,Belgium.

46. Lemercier, C.A., Lightsey, W.D., and Kelley, H.J., "Terminal Transient for Optimal Dash", Presentation in the Last-Minute Results Session, Seventh International Conference on Analysis and Optimization of Systems, Antibes, France, June 25-27, 1986.

47. Seywald, H., "Range-Optimal Trajectory for a Supersonic Aircraft", Thesis, Technische Universität München, 1984.

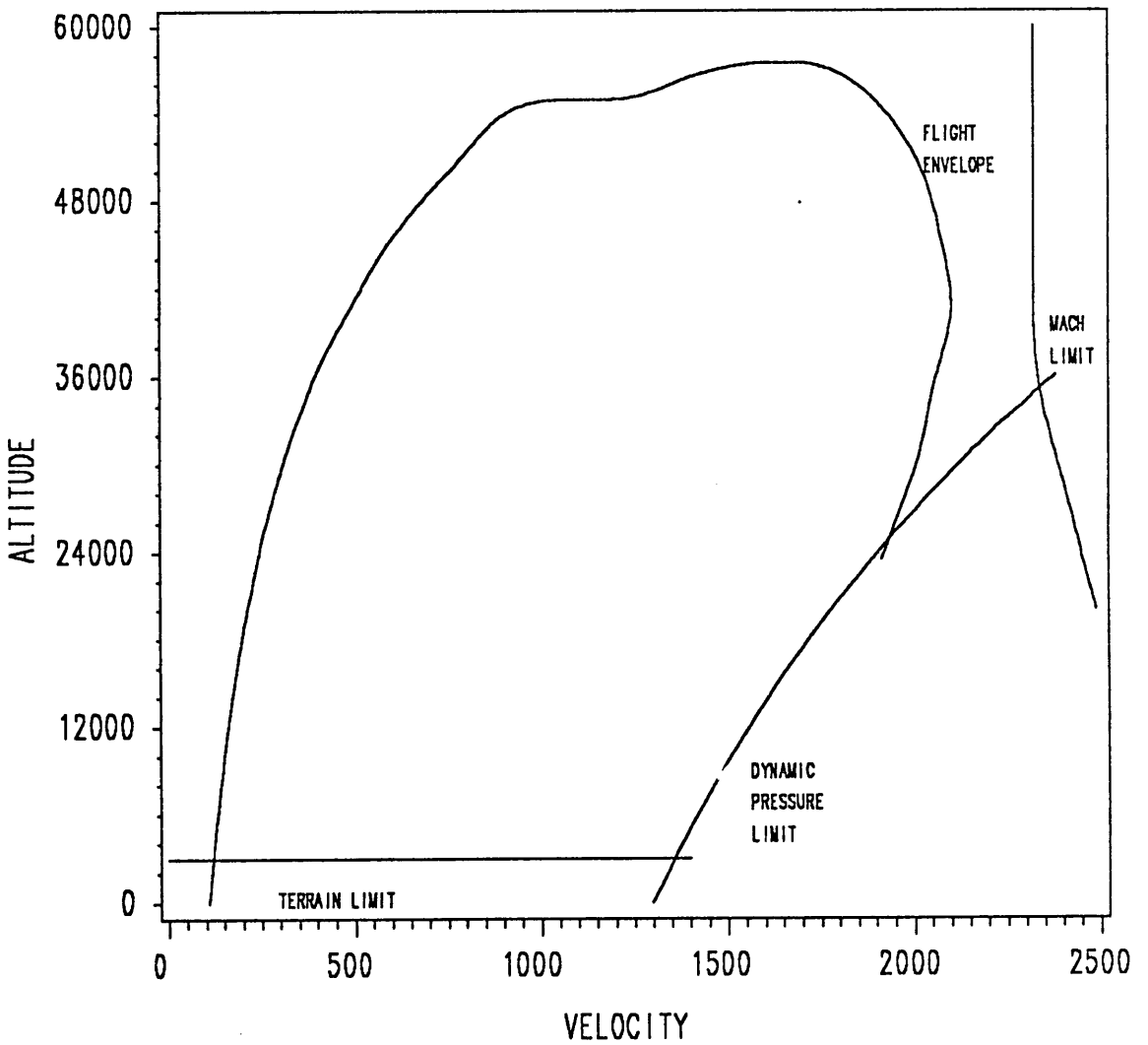

Figure 1. Flight Envelope and Constraints

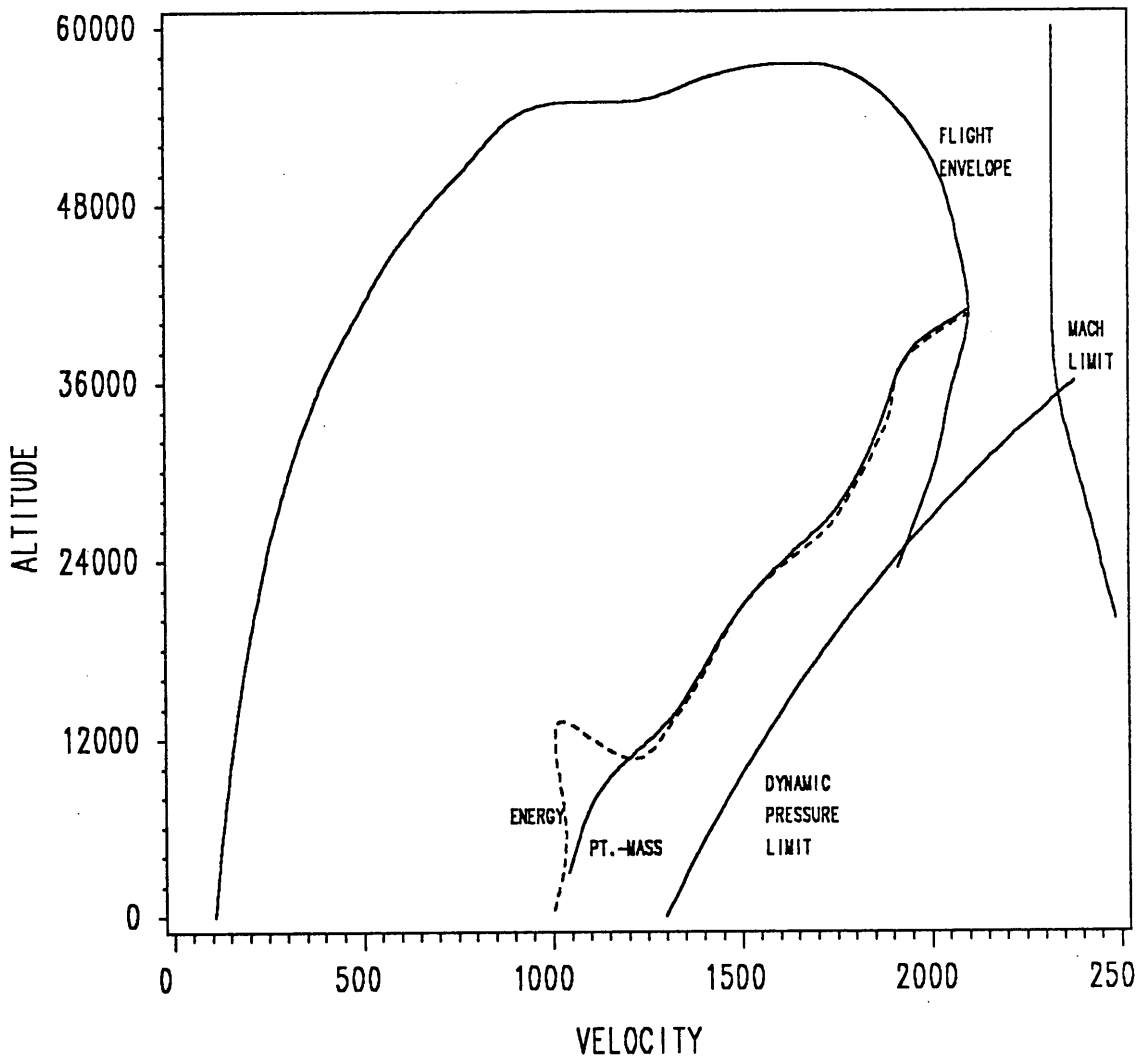

Figure 2. Energy and Point-Mass Solutions

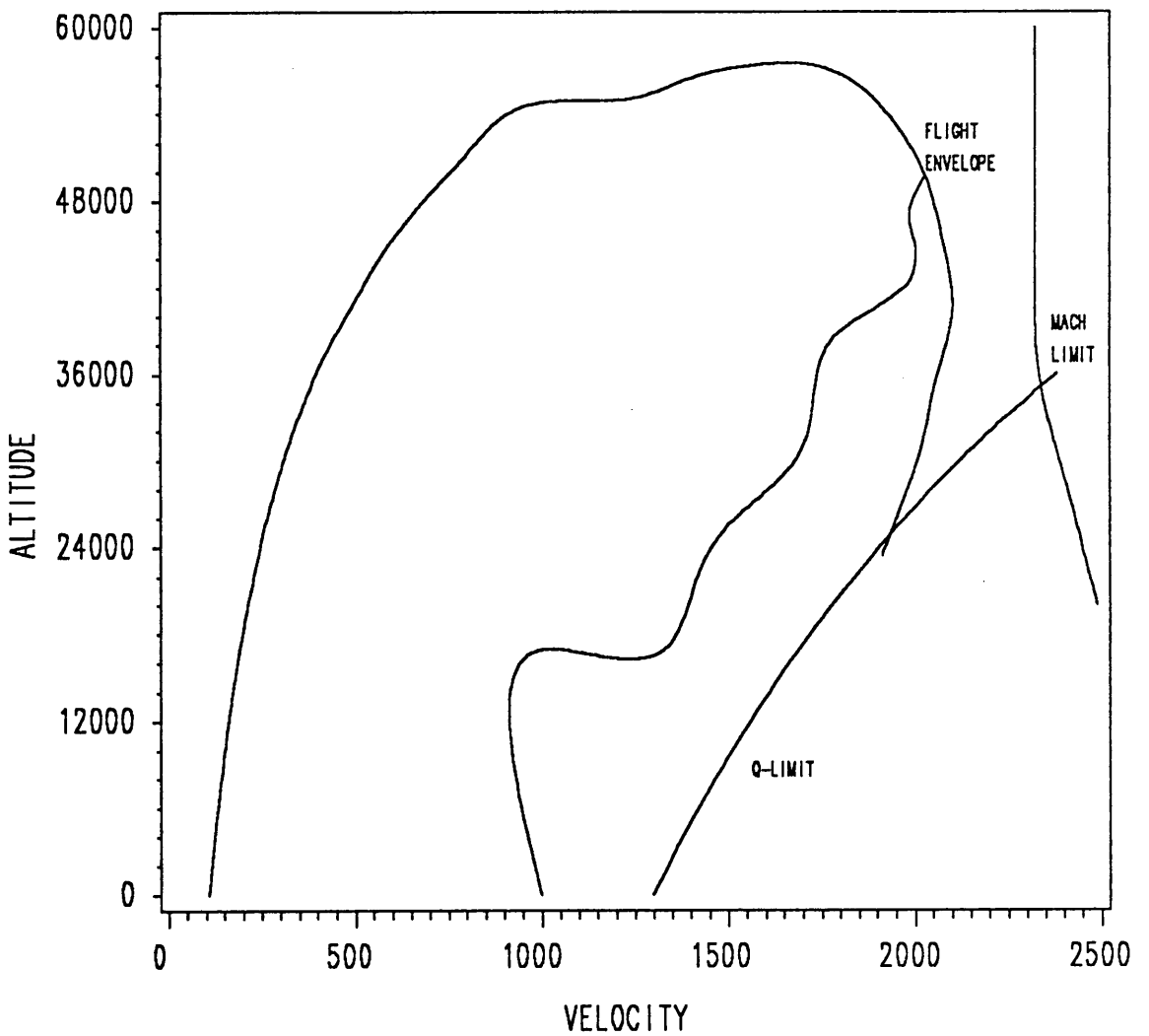

Figure 3. Energy Climb

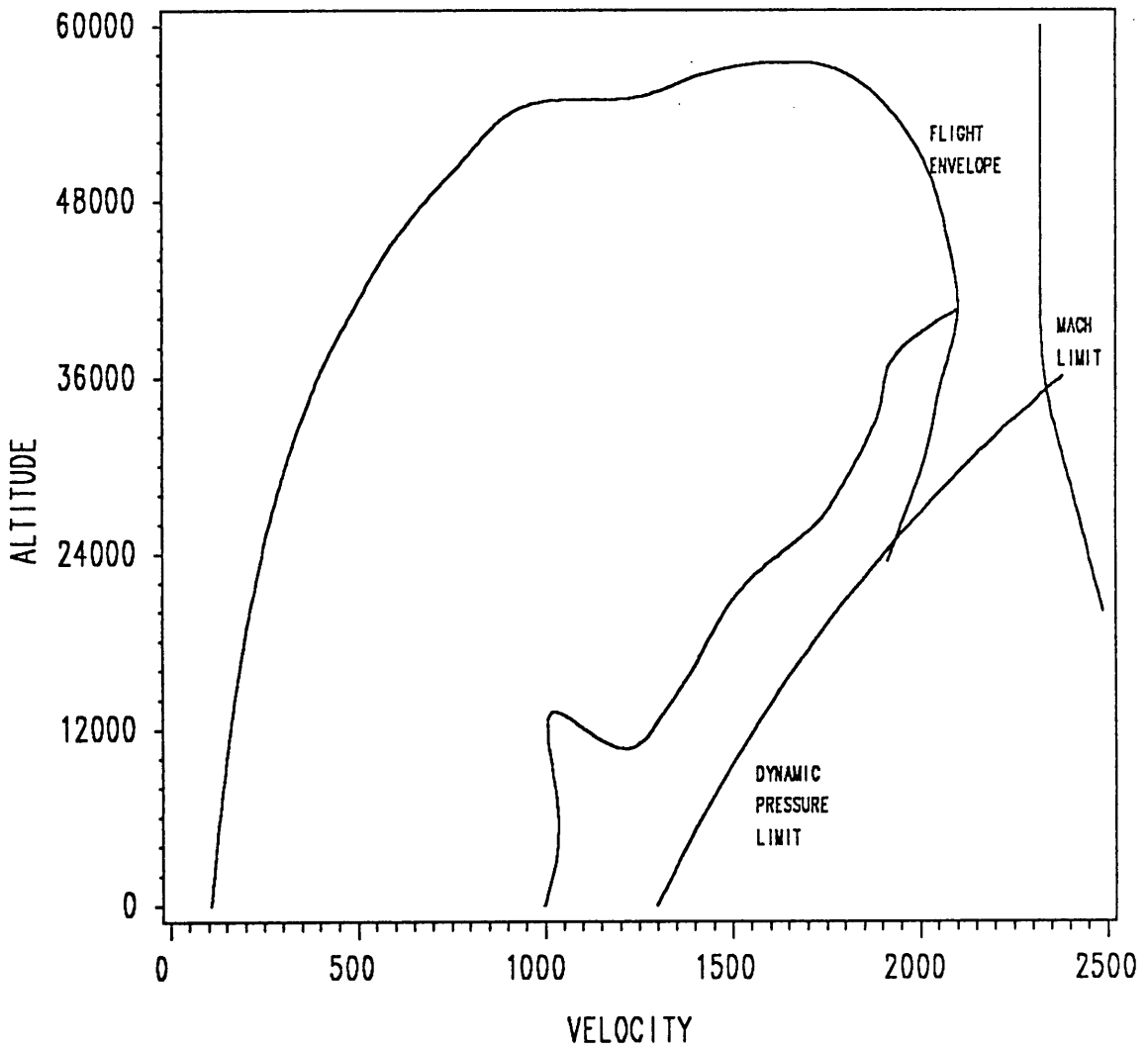

Figure 4. Energy Solution to Dash Point

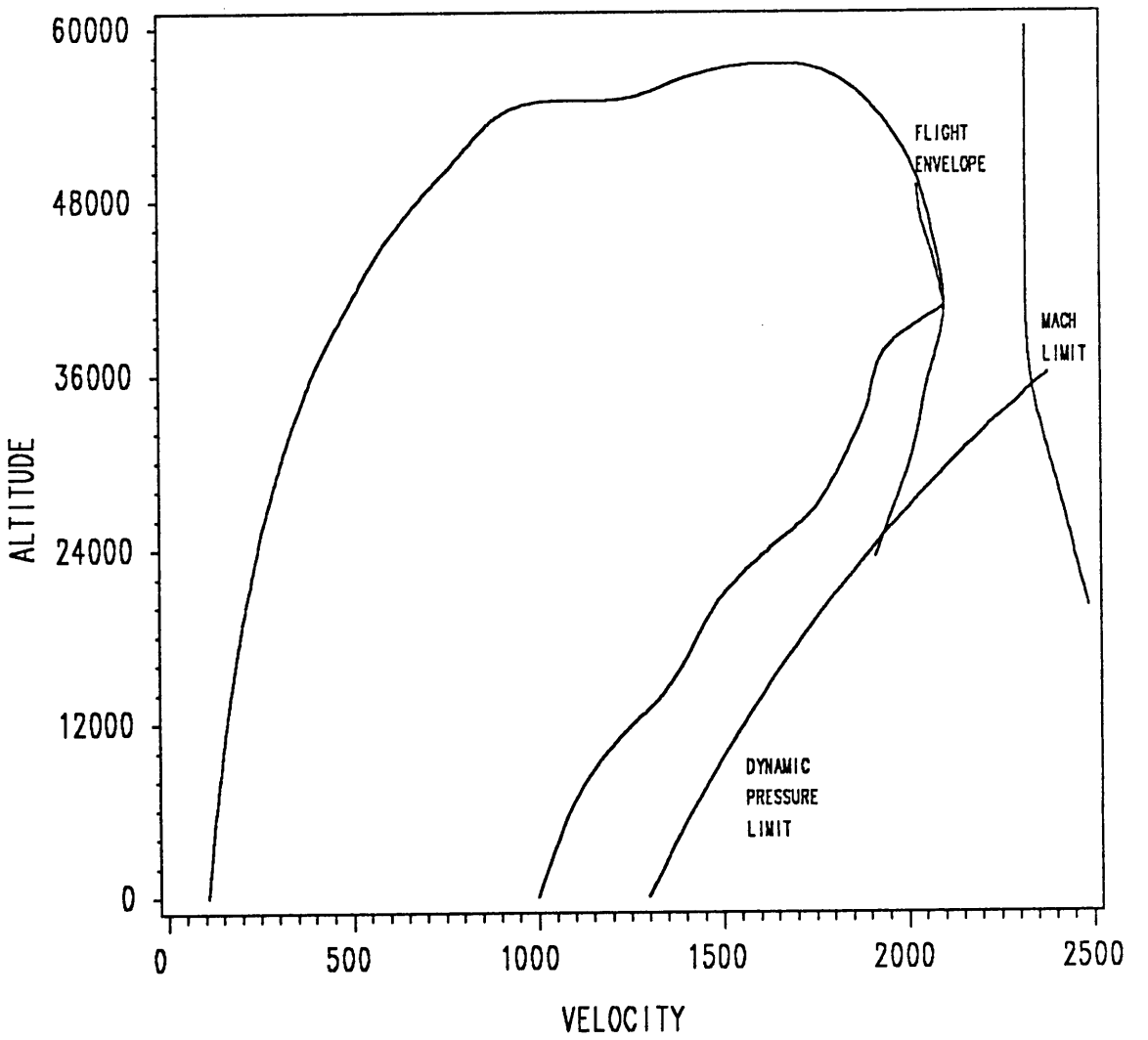

Figure 5. Dash to High-Energy-Point Transition

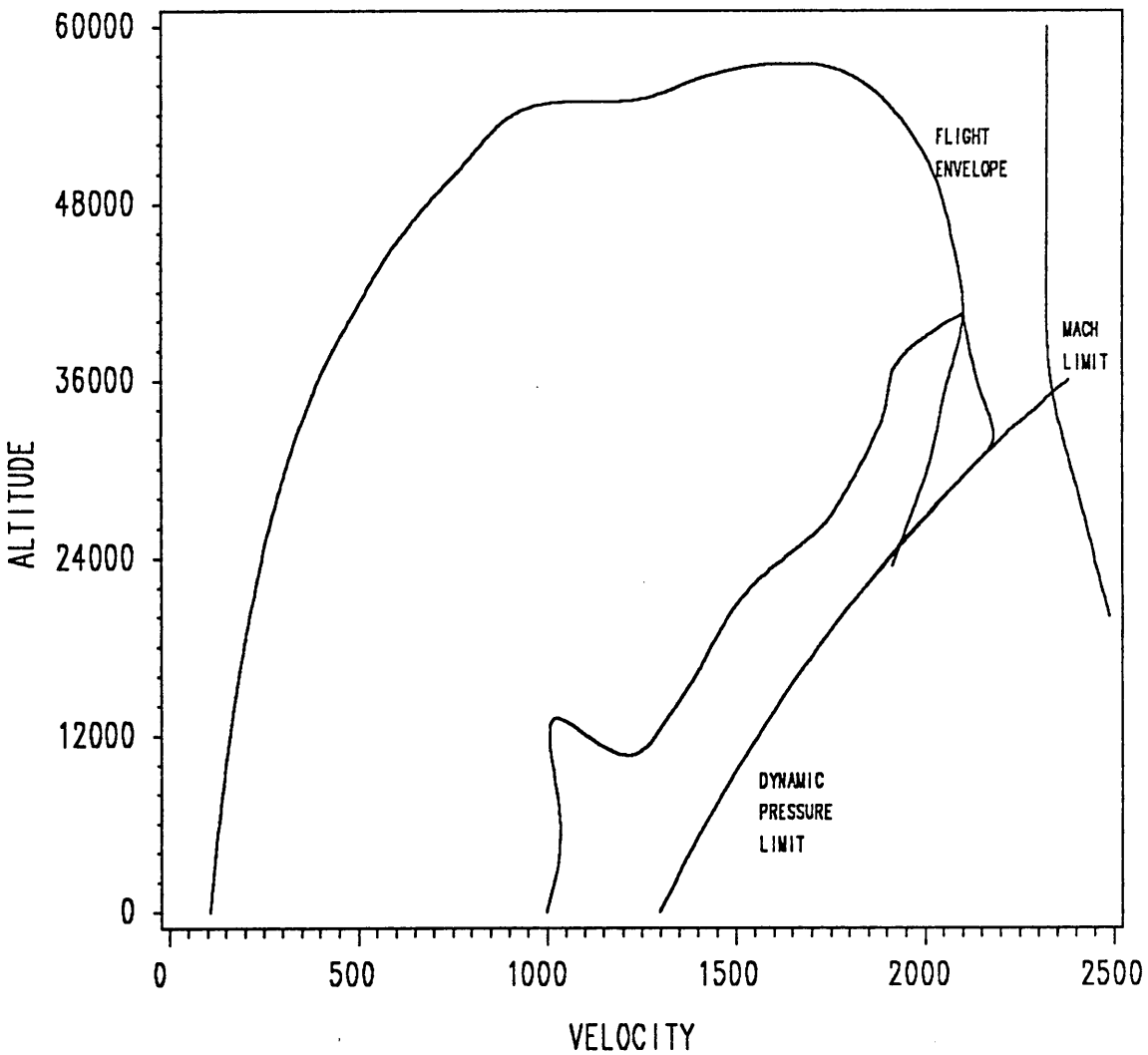

Figure 6. Energy Solution with Terminal Transient

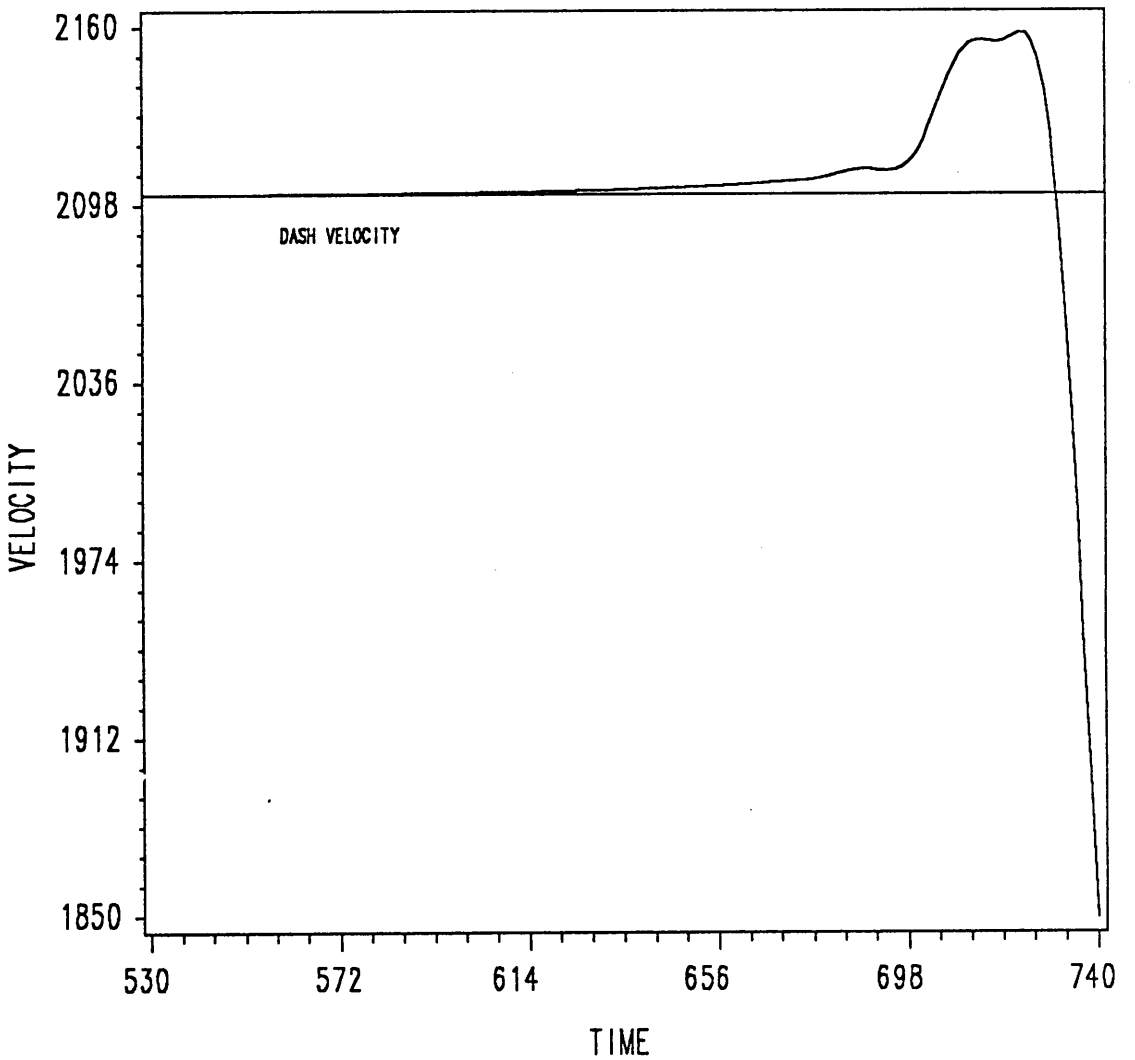

Figure 7. Velocity-Time History

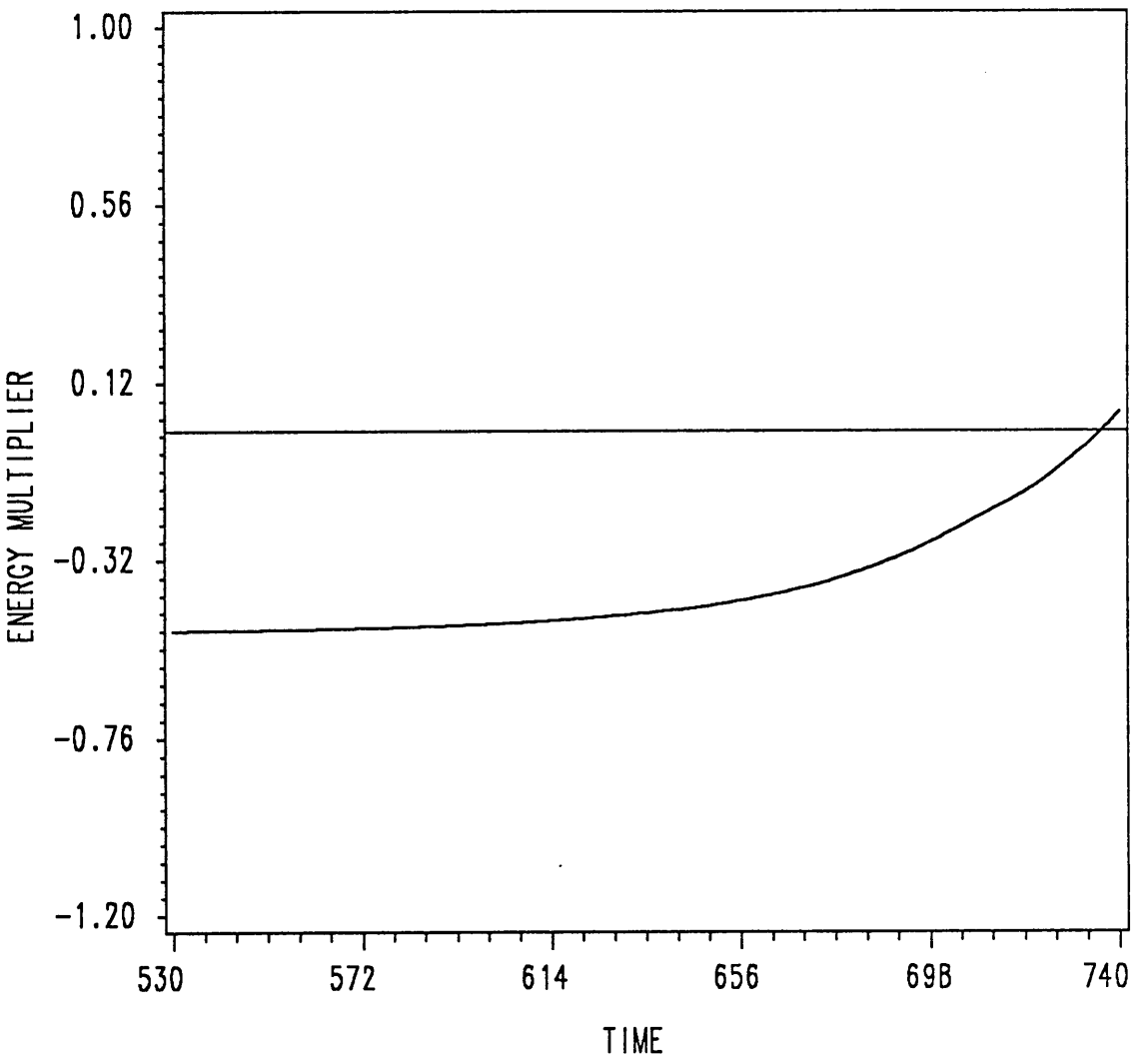

Figure 8. Energy Multiplier Time History

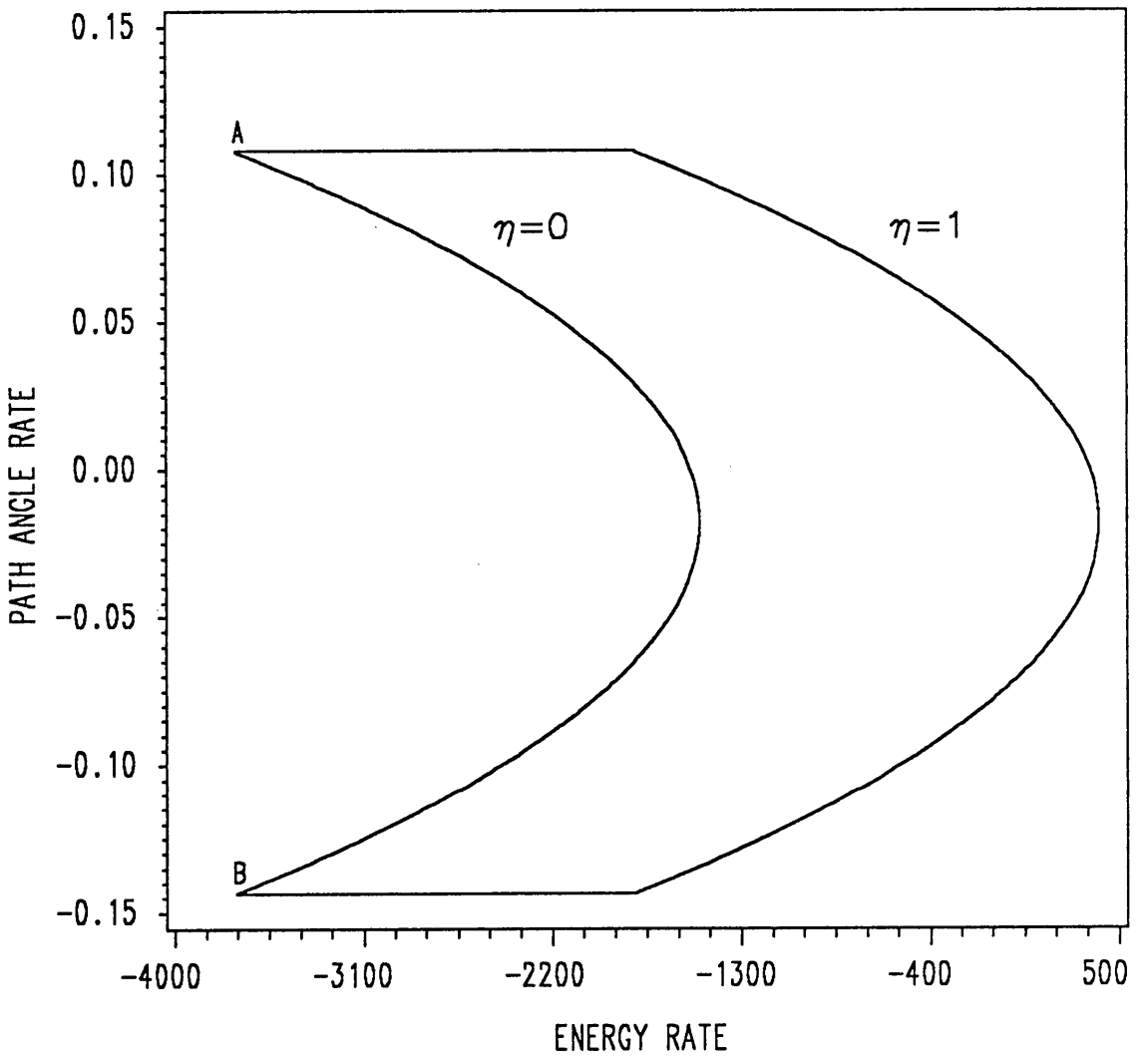

Figure 9. Hodograph Figure for Point-Mass Model

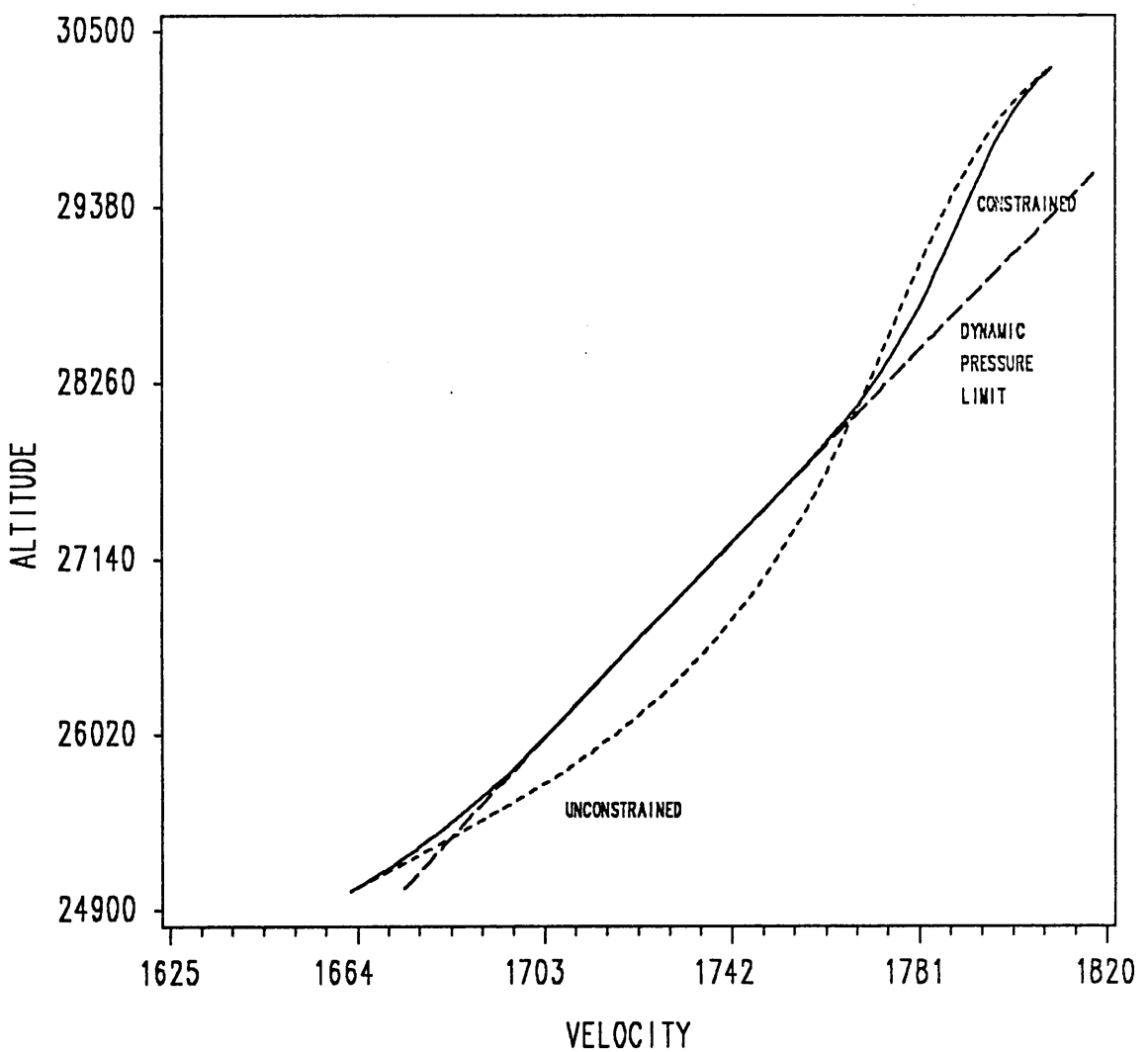

Figure 10. Constrained vs. Unconstrained Solution

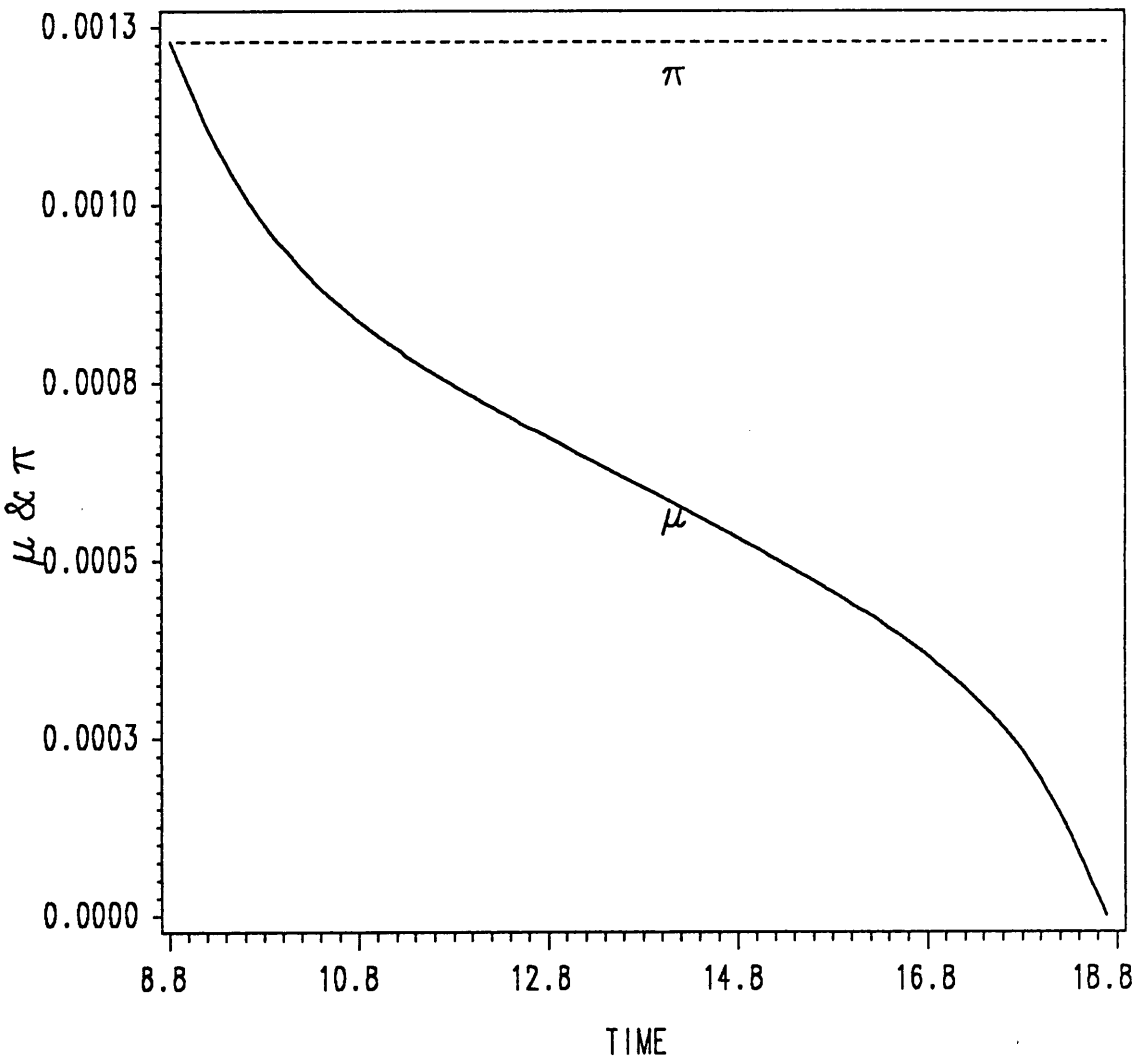

Figure 11. μ and π Time Histories on Constraint

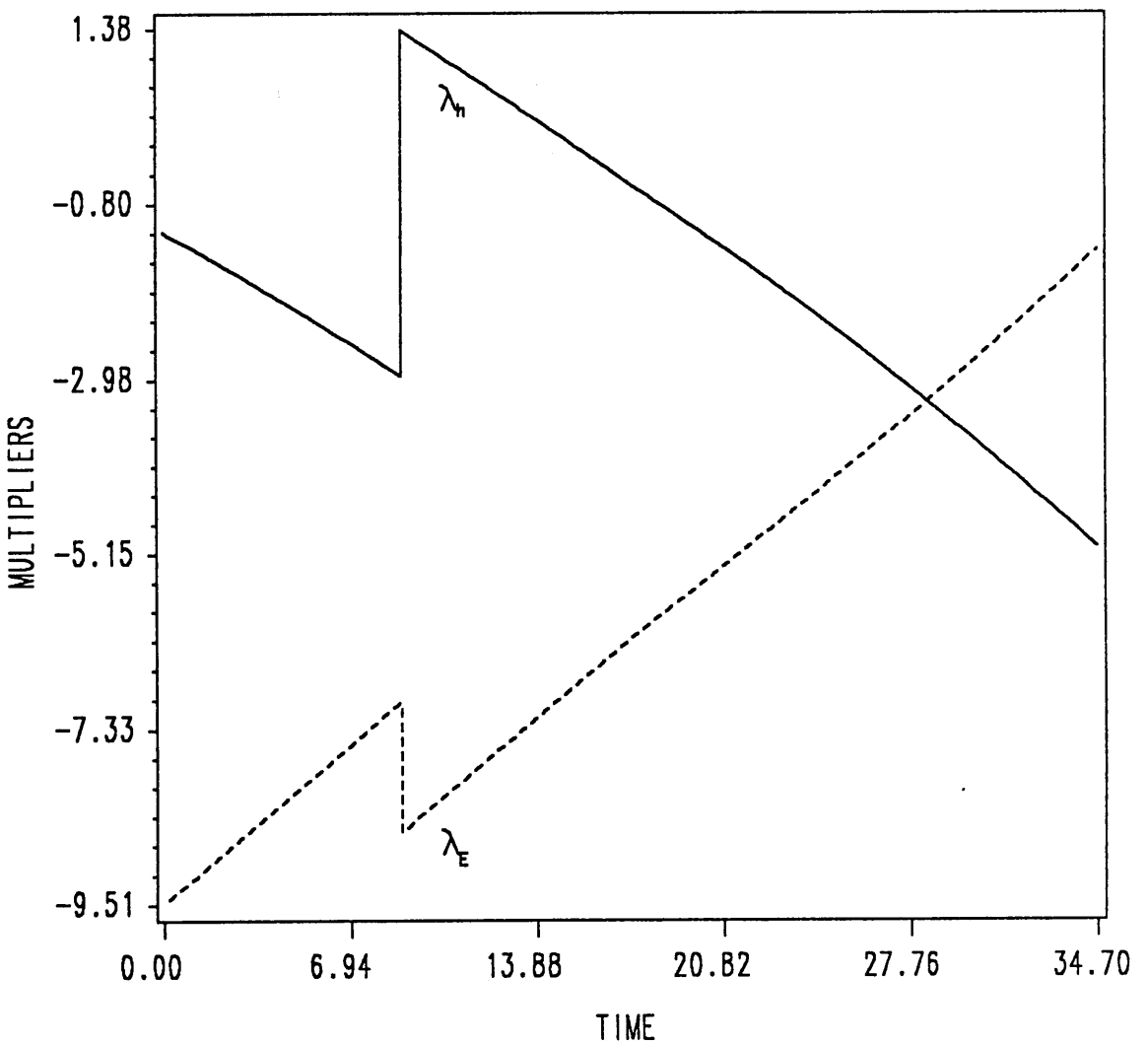

Figure 12. Time History of Energy and Altitude Multipliers

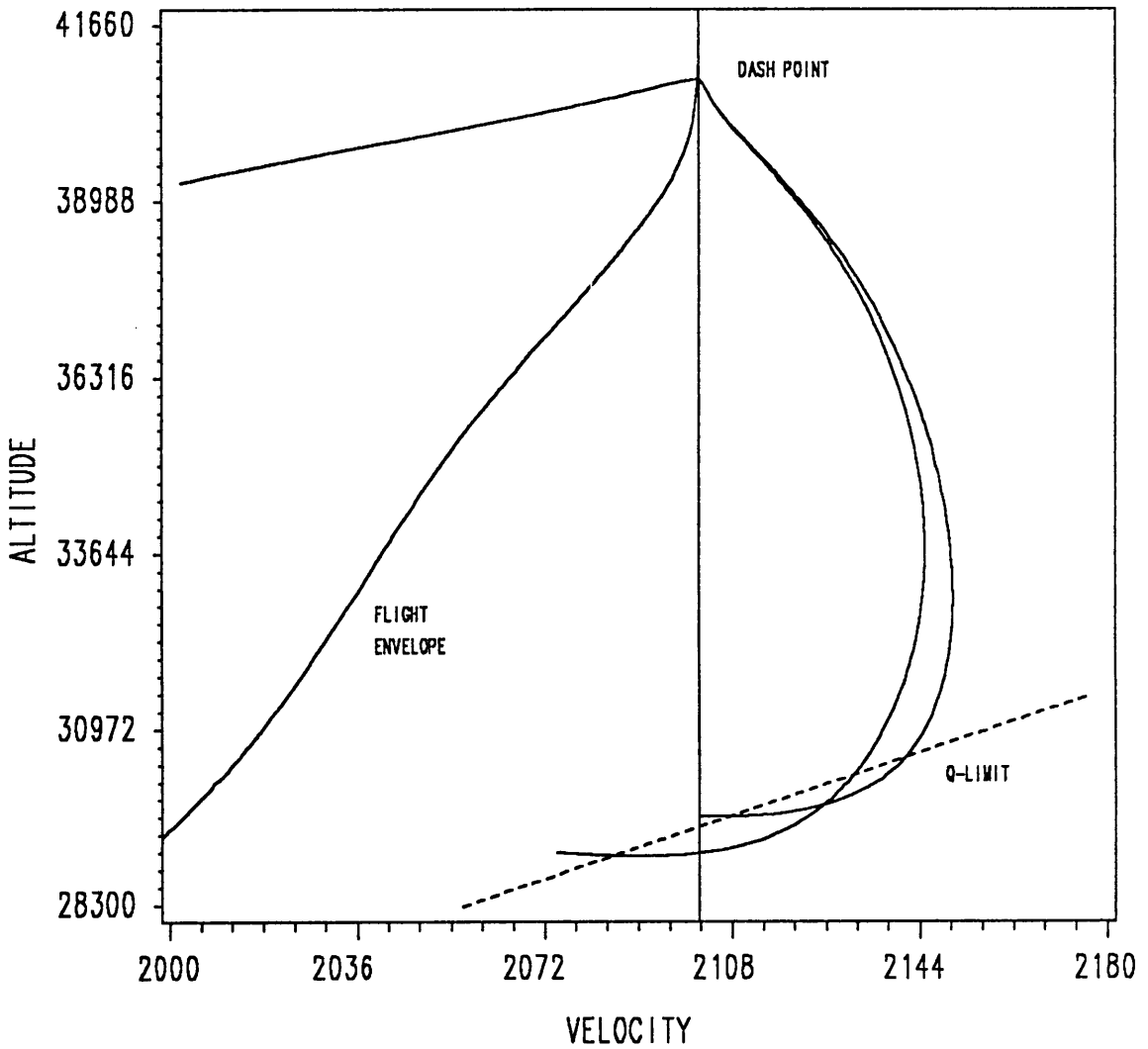

Figure 13. Unconstrained Solutions

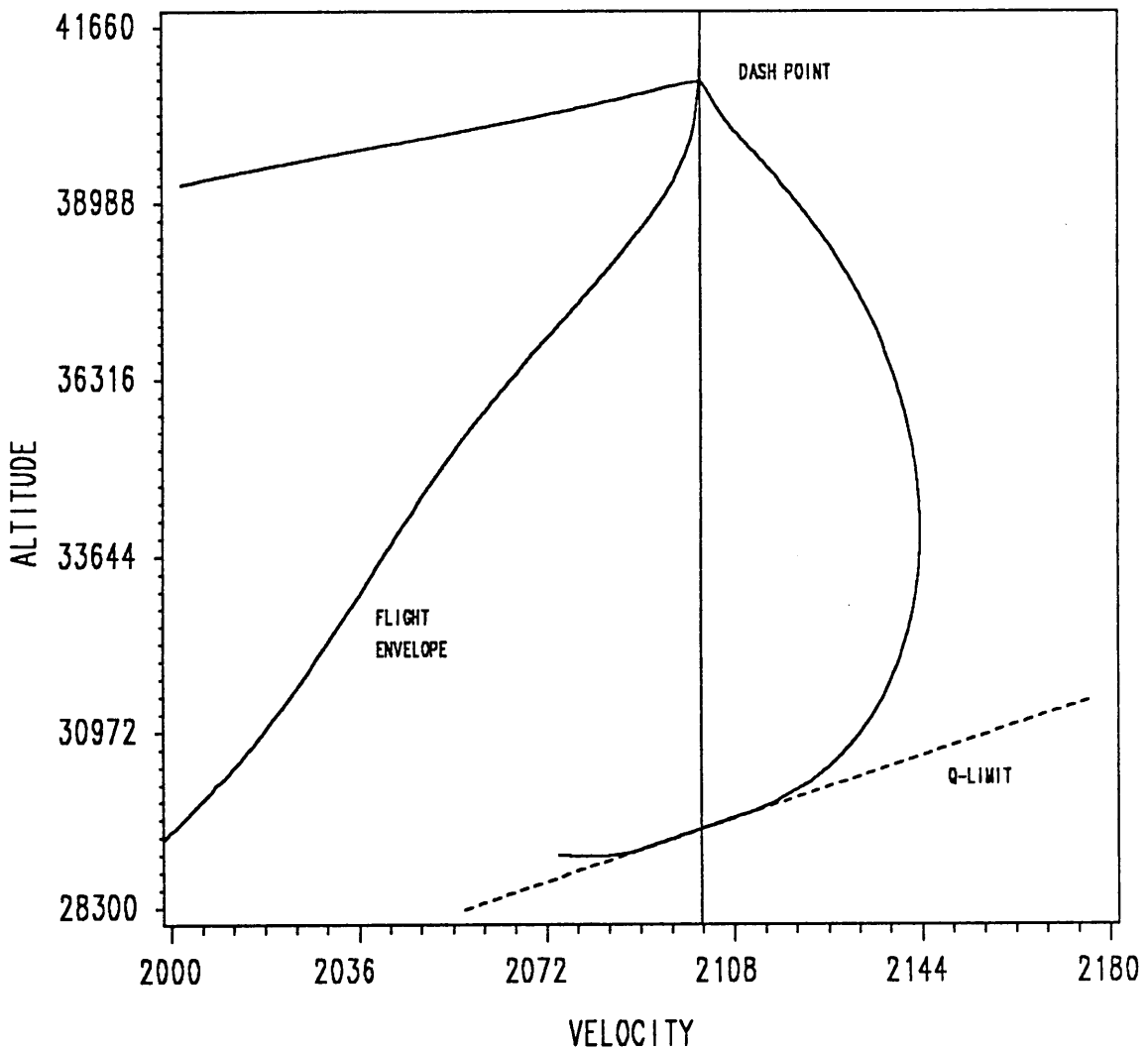

Figure 14. Constrained Solution

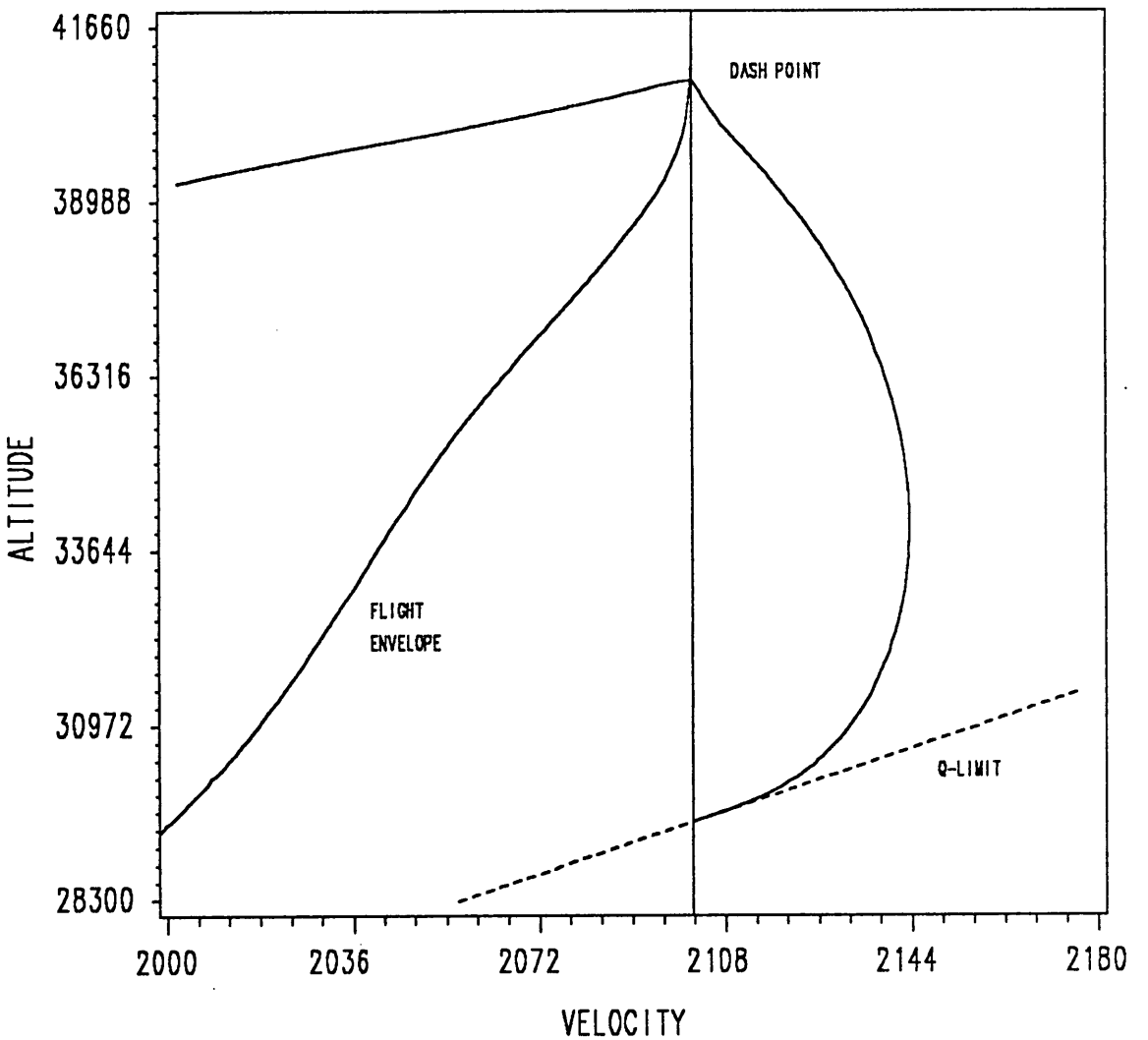

Figure 15. Constrained Path Terminating at Throttle Switch Time

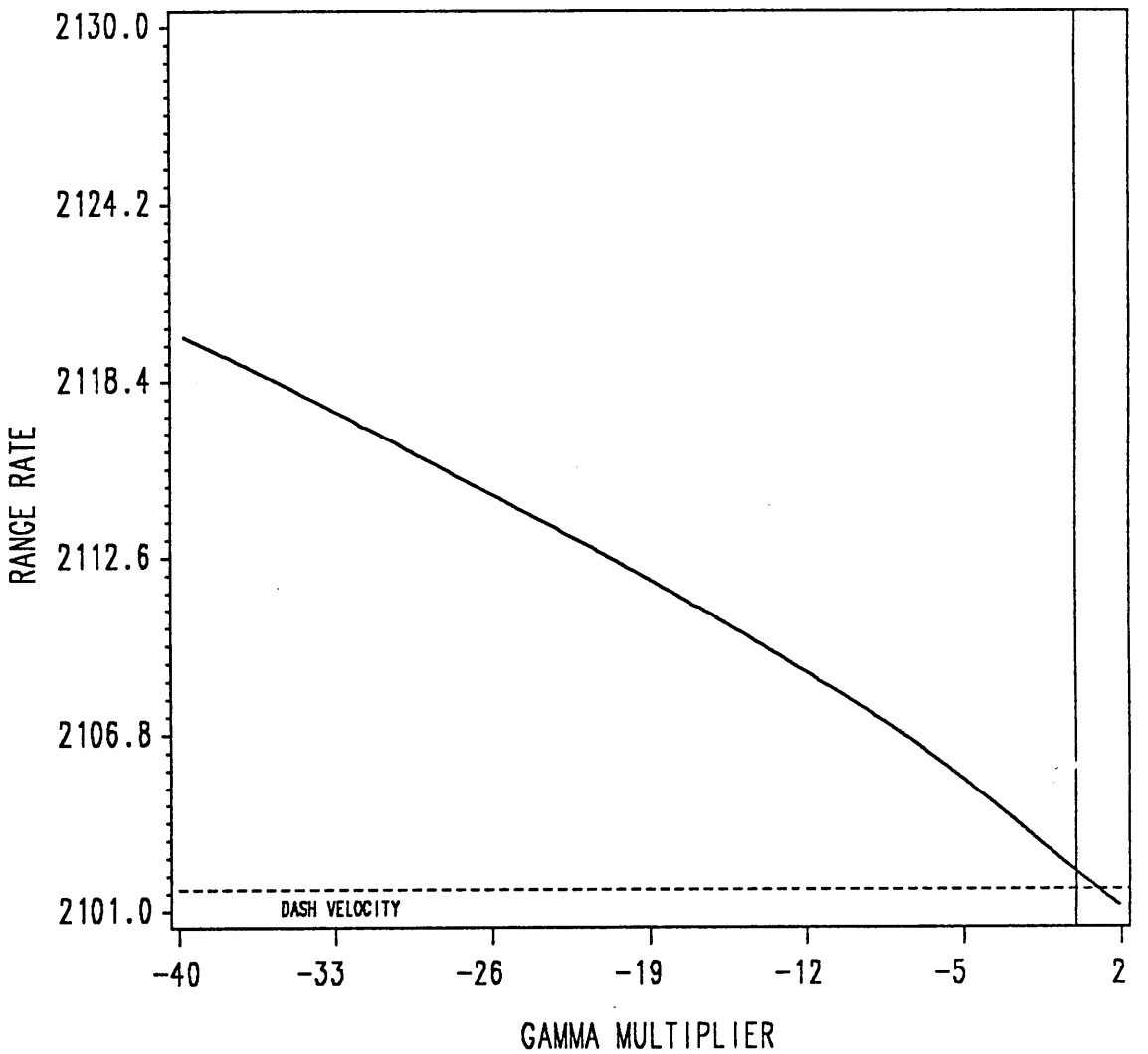

Figure 16. Range Rate vs. Path Angle Multiplier Along Constraint

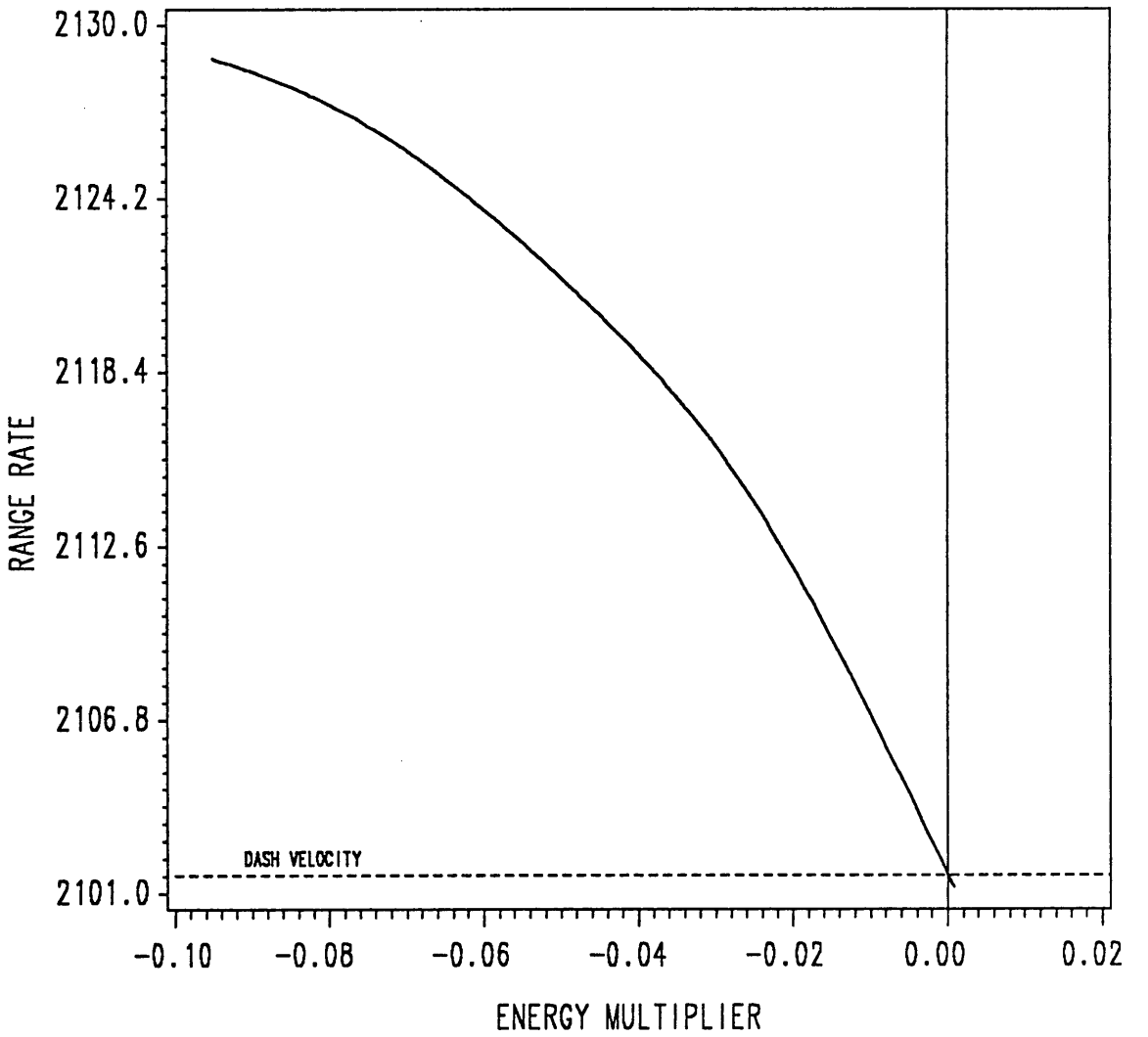

Figure 17. Range Rate vs. Energy Multiplier

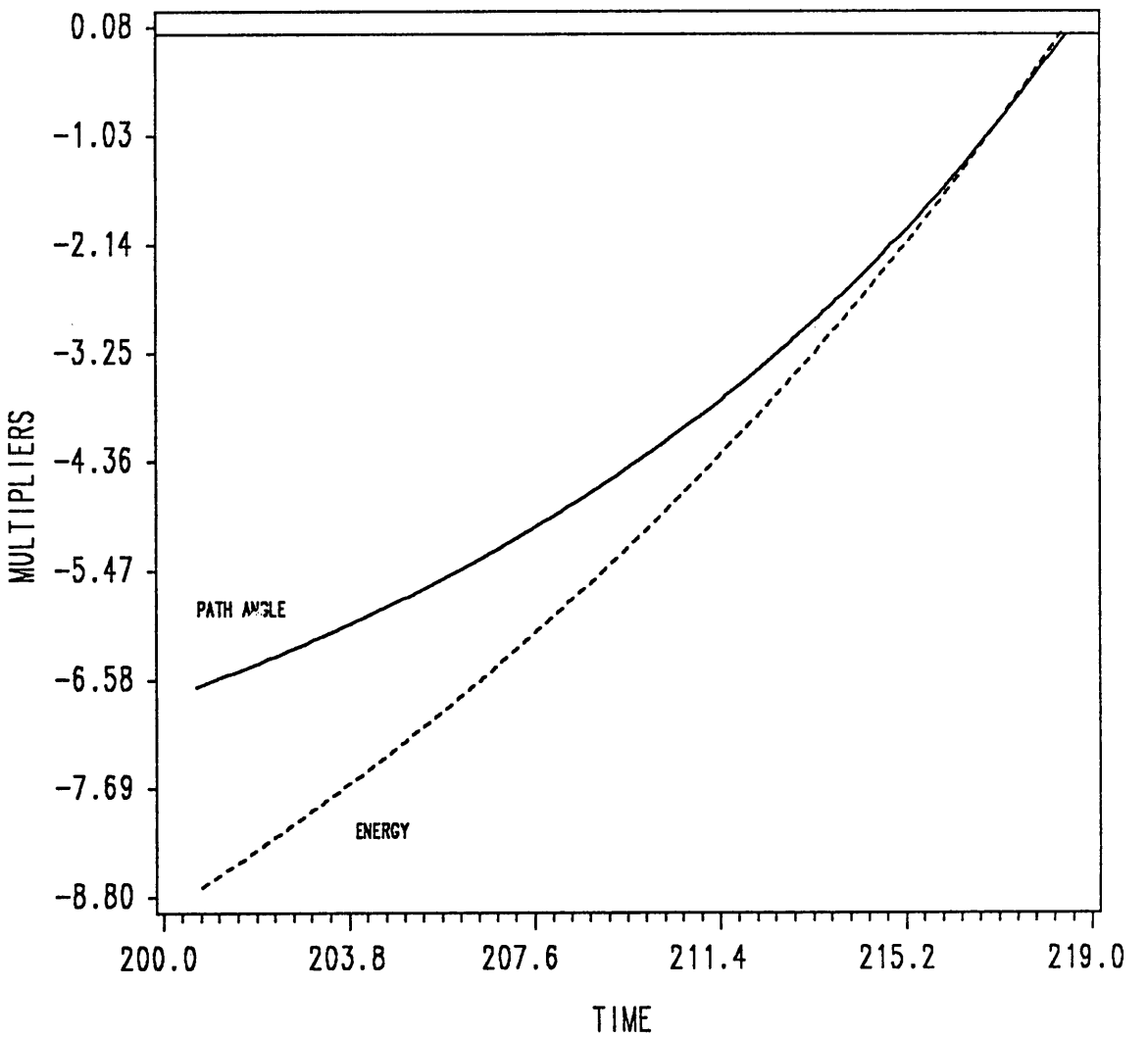

Figure 18. Time Histories of λ_γ and λ_E (unconstrained)

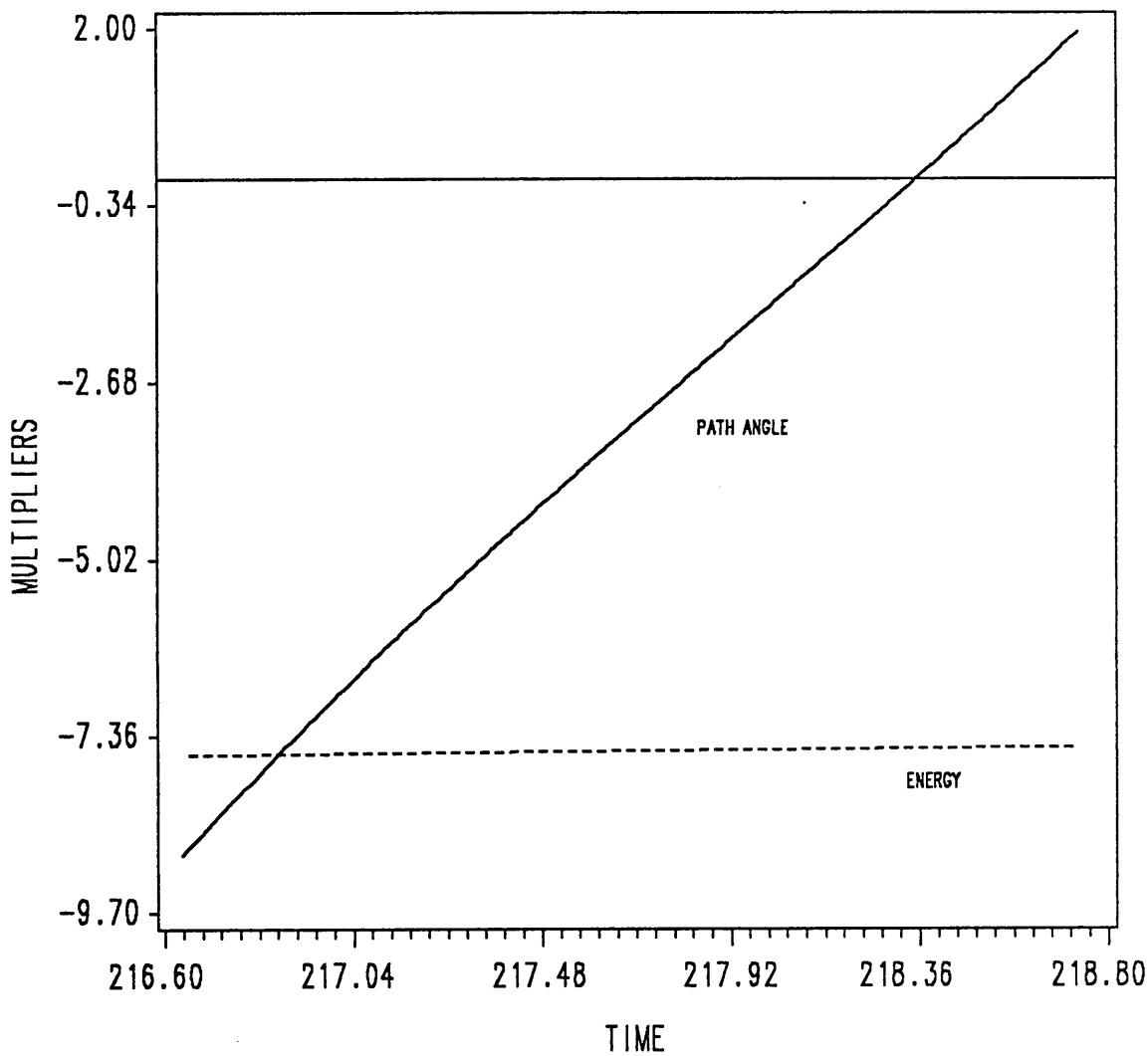

Figure 19. Time Histories of λ_γ and λ_E (constrained)

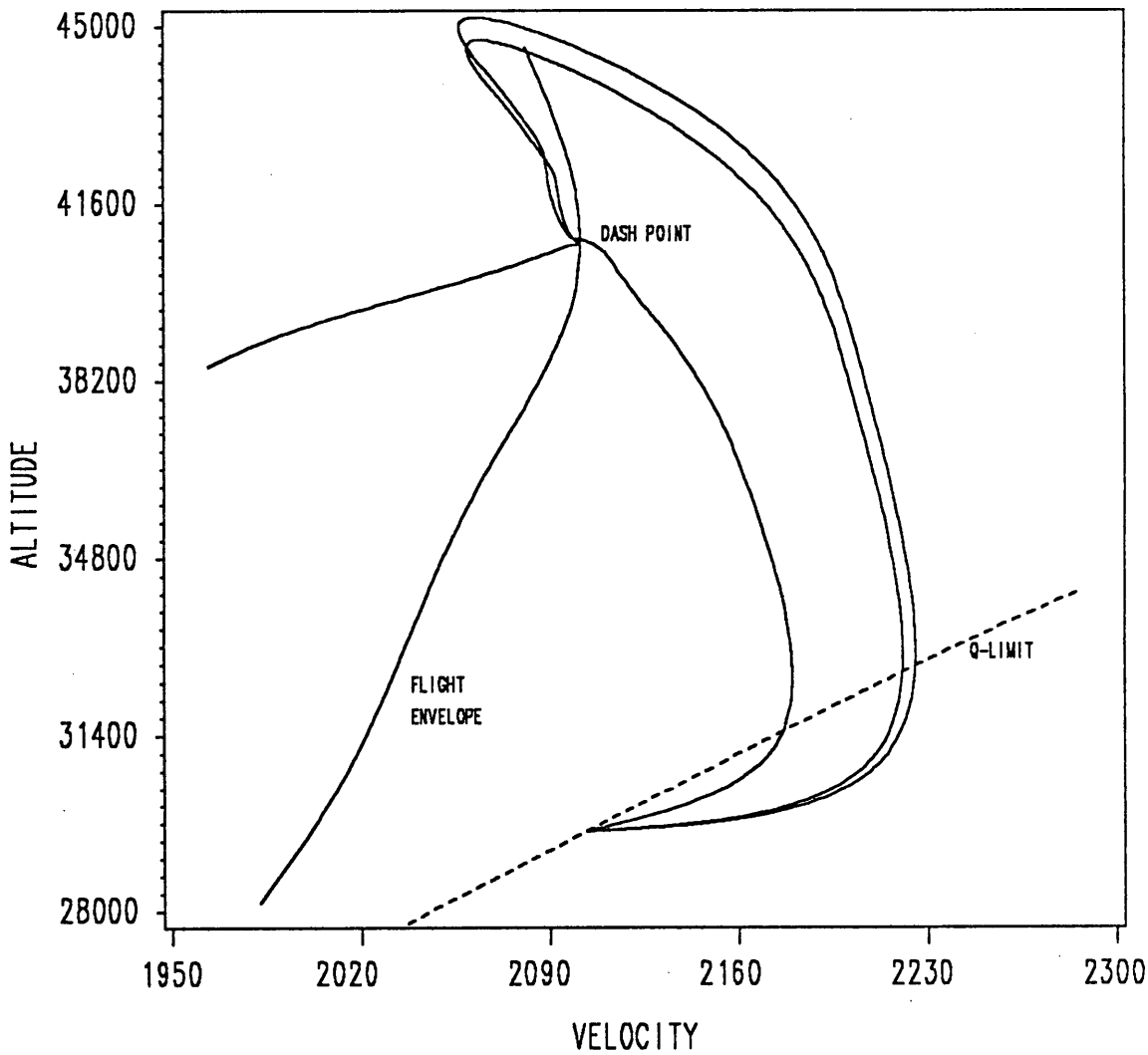

Figure 20. Unconstrained Paths to Various Final Path Angle Values

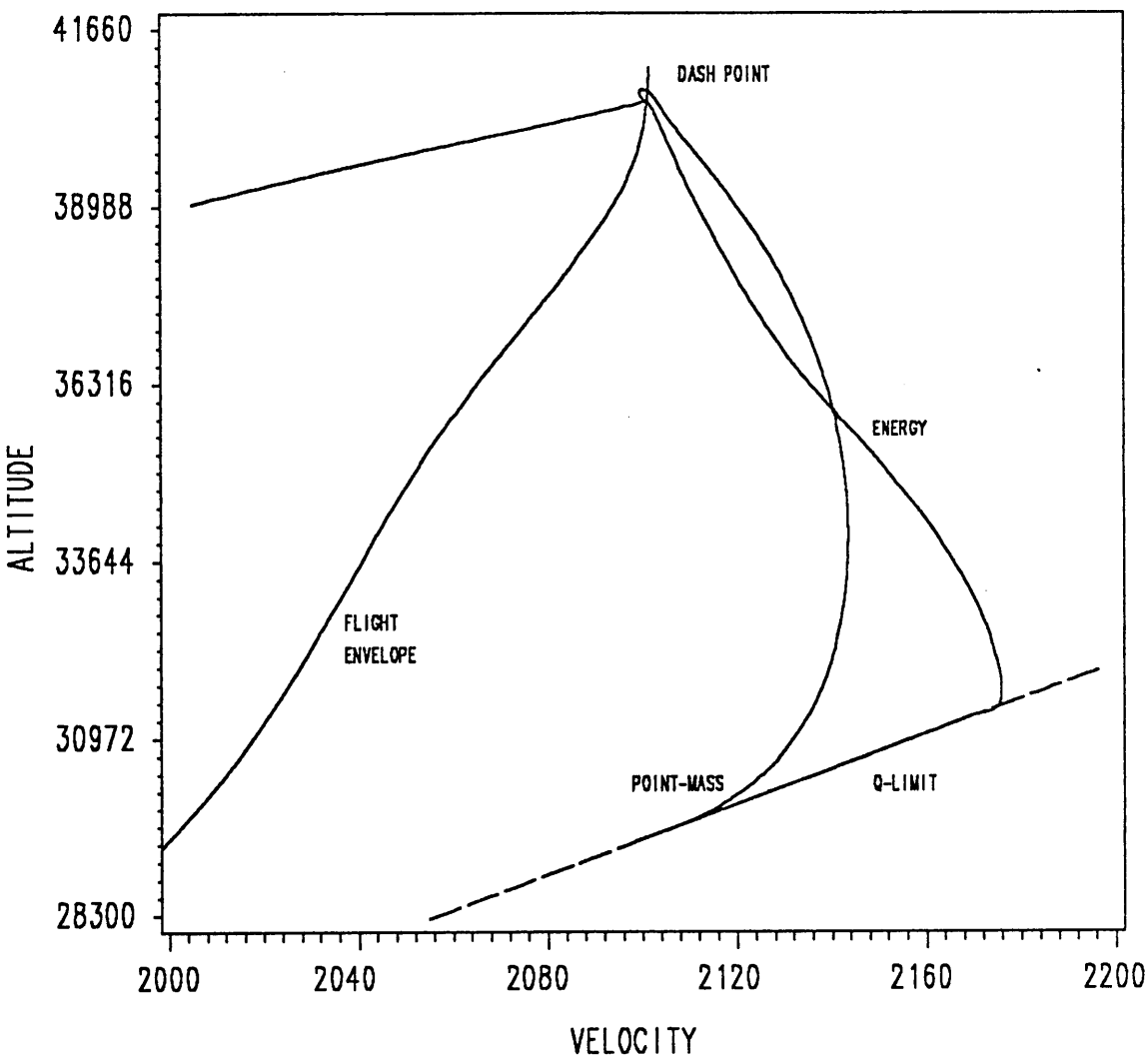

Figure 21. Energy and Point-Mass Terminal Transient Maneuvers

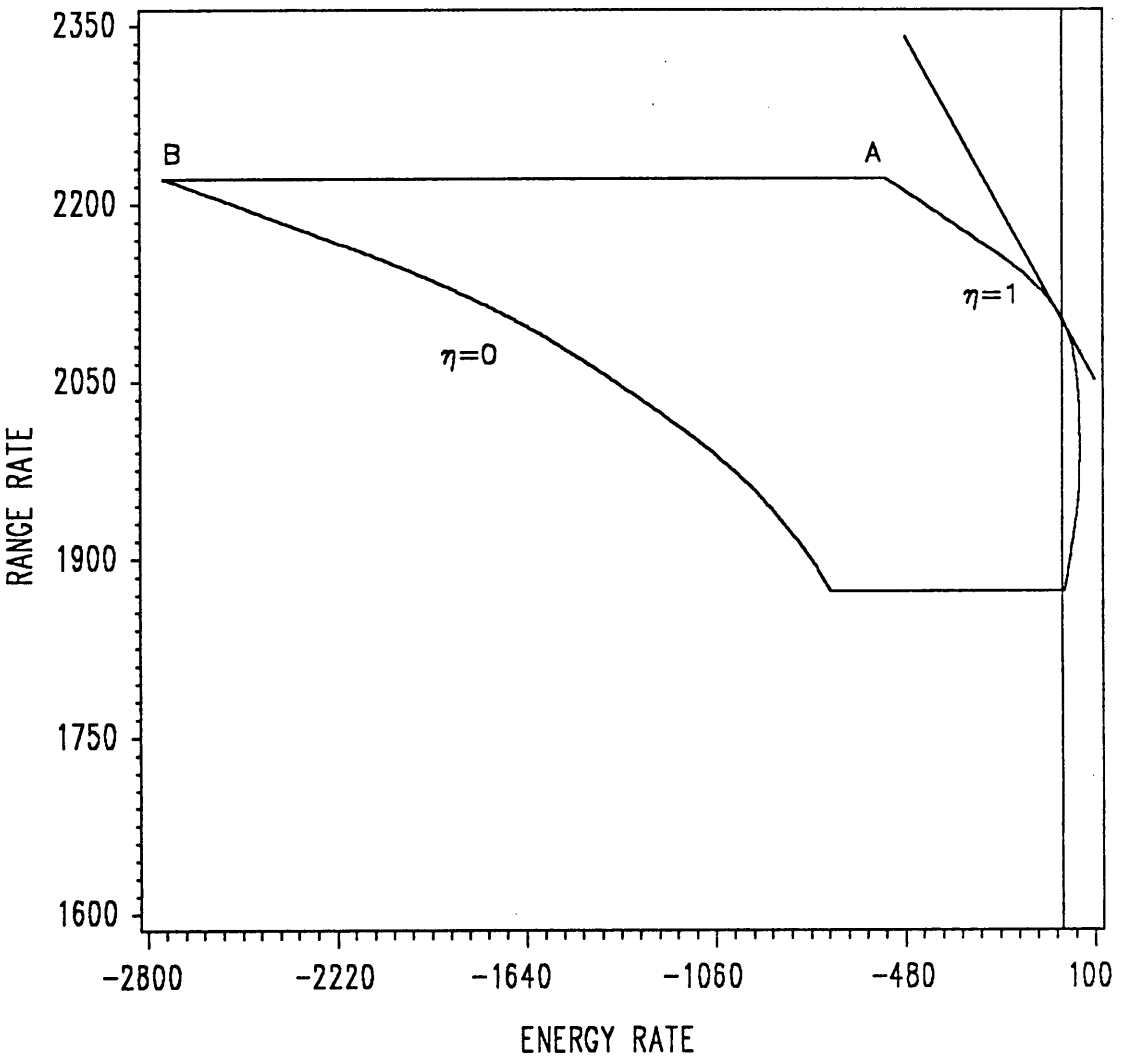

Figure 22. Hodograph For Energy Model Formulation

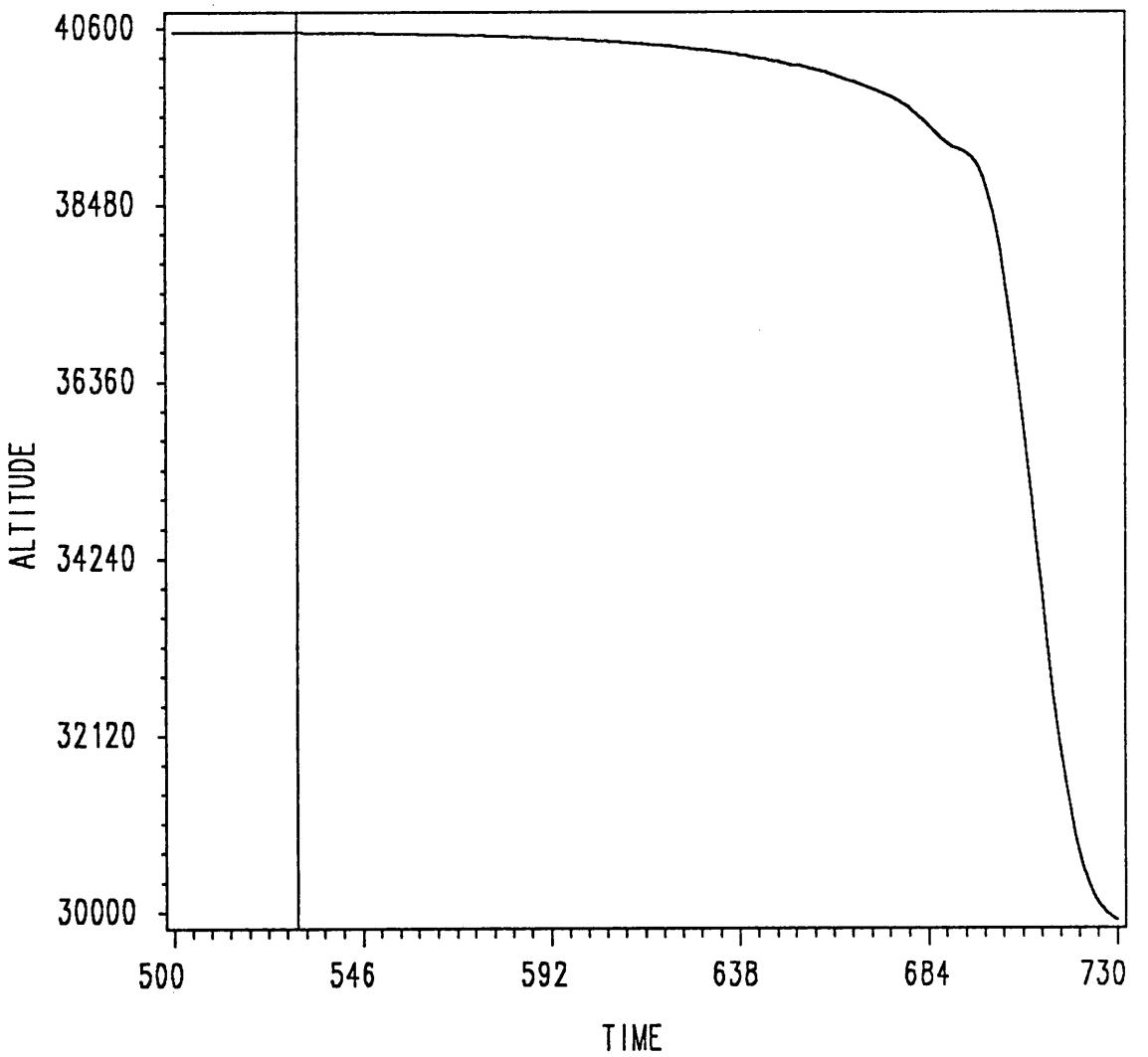

Figure 23. Altitude Time-History Near Dash-Point

The vita has been removed from the scanned document